

**Laser-based Ultrasonic Assisted Low Speed
Micro Milling of Super Alloys**



Author

Yadullah Haidary

MS (Design and Manufacturing Engineering)

00000318519

Supervisor

Dr. Syed Hussain Imran Jaffery

Department of Design and Manufacturing Engineering
School of Mechanical and Manufacturing Engineering (SMME)
National University of Sciences & Technology (NUST)

Islamabad, Pakistan

(August 28, 2023)

Thesis Acceptance Certificate

Certified that final copy of MS Thesis Written by Mr. Yadullah Haidary (Registration No: 00000318519), of Design and Manufacturing Engineering (School/College/Institute) has been vetted by undersigned, found complete in all respects as per NUST Statutes/ Regulations, is free of plagiarism, errors and mistakes and is accepted as partial fulfillment for award of MS/MPhil Degree. It is further certified that necessary amendments as pointed out by GEC members of the scholar have also been incorporated in the said thesis.

Signature: _____

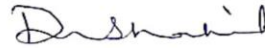


Dr. Syed Hussain Imran
Professor
School of Mechanical and
Manufacturing Engineering
(SMME) NUST, Islamabad

Name of the supervisor: Dr. Syed Hussain Imran

Date: 24-08-23

Signature (HOD): _____



Date: 25-08-23

National University of Science and
Technology
MASTER THESIS WORK

We hereby recommended that the dissertation prepared under our supervision by **Yadullah Haidary** (00000318519) titled: "**Laer-Based Ultrasonic Assisted Low Speed Micro Milling of Super Alloys**" be accepted in partial fulfillment of the requirements for the MS Design and Manufacturing Degreee.

Examination Committee Members

1. Name: Dr. Muhammad Salman Khan

Signature: 

2. Name: Mr. Ahmad Waqar Tehami

Signature: 

Supervisor Name: Dr. Syed Hussain Imran Jaffery


Signature: 

Date: _____
Dr. Syed Husain Imran
Professor
School of Mechanical and
Manufacturing Engineering
(SMME) NUST, Islamabad


Head of Department

Date: 24-08-23

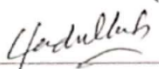
COUNTERSIGNED


Dean/Principal

Date: 25-08-23

Declaration

I certified that this research work titled "**Laer-Based Ultrasonic Assisted Low Speed Micro Milling of Super Alloys**" is my own work. The work has not been presented elsewhere for assessment. The material that has been used from other sources it has been properly acknowledge/referred.


Mr. Yadullah Haidary

COPYRIGHT STATEMENT

Copyright in text of this thesis rests with the student author. Copies (by any process) either in full, or of extracts, may be made only in accordance with instructions given by the author and lodged in the Library of SMME, NUST. Details may be obtained by the Librarian. This page must form part of any such copies made. Further copies (by any process) may not be made without the permission (in writing) of the author.

The ownership of any intellectual property rights which may be described in this thesis is vested in SMME, NUST, subject to any prior agreement to the contrary, and may not be made available for use by third parties without the written permission of SMME, NUST, which will prescribe the terms and conditions of any such agreement.

Further information on the conditions under which disclosures and exploitation may take place is available from the Library of SMME, NUST Islamabad.

ACKNOWLEDGEMENT

This Thesis work has been done at School of Mechanical and Manufacturing Engineering (SMME) at NUST, Islamabad under the project “*Laer-based Ultrasonic Assisted Low Speed Micro Milling of Super Alloys*” and is submitted in partial fulfillment of the requirements for the degree of Master of Science program in Design and Manufacturing (DME) at SMME, NUST University.

I am grateful to my Project Supervisor **Dr. Syed Hussain Imran Jaffery** for his constant guidance, support, friendly behavior and encouragement for working hard made me able to achieve this milestone. His critical views were the most helpful thing while doing this dissertation work and the project.

Besides my advisor, I would like to thank the rest of my thesis committee: **Dr. Muhammad Salman Khan** and **Mr. Ahmed Waqar Tehami** for their insightful comments and encouragement, but also for the hard question which incited me to widen my research from various perspectives.

I also acknowledge the help of **Engr. Daniyal Zahid** and thank him for guiding me along the right path throughout my research. I shall not forget CNC machine operators **Mr. Waseem, Mr. Akseer** along with **Laser and Advance Microscopy Lab.** operators **Mr. Ansar** and **Mr. Umar** for making the working in the laboratory a joy.

Last but not the least, I would like to thank my family for their never-ending support and encouragement through very difficult times to complete research work. Especially my **mother, my late father and my siblings** who prayed for me every second.

I am thankful to my class mates for their assistance, advices and group discussions. Their help directly or indirectly was really supportive for this task completion.

DEDICATION

*To my Beloved
Parents and Family
Members, without
whom none of my
success would have
been possible*

&

*To my Respected Teachers,
Who acted like compass
that activated the magnets of
curiosity, knowledge and wisdom in me*

&

*Engineer **Rafi-u-Shan Ahmed** for
having Believe in me and keep me
Motivated thorough out my research*

ABSTRACT

Inconel-718 is a nickel-based super alloy with exceptional mechanical properties; including high yield, creep-rupture, and high tensile strength at temperatures up to 977 K. Along with its frequent uses in high temperature fasteners and bolts, and high-speed aircrafts' parts such as spacers, wheels, buckets, and engines, Inconel-718 have also its applications in automotive, submarine and biomedical industries. Although this nickel-based alloy is an ideal material for high temperature and high corrosive environment, it is difficult to handle while machining it. To improve the machinability of the alloy as compared to the conventional micro milling, an experimental setup has been designed using laser-based ultrasonic assisted low speed micro milling (LLUMM). This study focuses on low-speed ultrasonic milling of laser-cut constant-depth slots which are created on a workpiece of Inconel-718 using Laser Marking Machine. Effects of cutting parameters including cutting speed, feed rate, depth of cut, amplitude of tool vibration and tool coating surface roughness, tool wear and burr formation are investigated, using each factor at four different levels. Cutting tool's diameter is kept fixed at 0.5mm with uncoated and coated materials, including TiAlN, TiSiN, and nACo. A Design of Experiment technique, namely Taguchi L16 array, is used to create experiments. Experimental data is statistically analysed to identify the best and worst set of parameters for achieving the desired results. Optimization of individual response variables is carried out using signal to noise ratios, with the help of Minitab-21, while multi-objective optimization uses Weighted Grey Relational Grades (W-GRG) in which Grey Relational Analysis is coupled with Principal Component Analysis (GRA-PCA). It has been revealed by validation experiments that LLUMM produces better results as compared to traditional micro milling.

Keywords: Inconel-718, LLUMM, Laser-Cut, Burr Formation, Weighted Grey Relational Grades, GRA-PCA.

Table of Contents

DECLARATION	Error! Bookmark not defined.
COPYRIGHT STATEMENT	Error! Bookmark not defined.
ACKNOWLEDGEMENT	Error! Bookmark not defined.
DEDICATION	Error! Bookmark not defined.
ABSTRACT	9
List of Figures	12
List of Tables	13
CHAPTER 1: INTRODUCTION	9
1.1 Research Motivation	16
1.2 Research Objectives.....	17
1.3 Research Scope	17
1.4 Areas of Application	18
CHAPTER 2: LITERATURE REVIEW	19
2.1 Hybrid Micro Machining	20
2.2 Laser-Based Ultrasonic Assisted Low Speed Micro Milling (LLUMM).....	21
CHAPTER 3: EXPERIMENTAL SETUP	22
3.1 Work Piece Material	22
3.2 Cutting Tools and Conditions	22
3.3 Split Type Lase Marking Machine	23
3.4 CNC Milling Machine with Ultrasonic Setup	25
3.5 Selection of Machining Parameters	26
3.6 Response Variables	27
3.7 Design of Experiments.....	28
CHAPTER 4: OPTIMIZATION OF INDIVIDUAL RESPONSES	31
4.1 Analysis of Variance.....	31

4.2 Surface Roughness.....	31
4.3 Tool Wear	34
4.4 Burr Formation.....	36
4.5 Mono-Objective Optimization	44
CHAPTER 5: MULTI OBJECTIVE OPTIMIZATION	46
5.1 Multi Response Optimization	46
5.2 GRA-PCA.....	47
5.3 Response Surface Methodology (RSM) and Regression Modelling (RM)	50
5.4 Regression Model Optimization	52
5.5 Result Validation	54
CHAPTER 6: CONCLUSION AND FUTURE RECOMMENDATIONS.....	55
6.1 Conclusion	55
6.2 Future Recommendations	56
References.....	57

List of Figures

Figure 1.1: Comparison of Different Material Removal Techniques.....	15
Figure 1.2: Comparison of Superalloys with Steel at High Temperature Environments	16
Figure 2.2: Machining Accuracy of Different Machining Techniques Over Time	19
Figure 2.3: Classification of Hybrid Micro Machining Techniques.....	20
Figure 3.1: Machined Slots on Inconel 718.....	22
Figure 3.2: Setup of Laser Machine.....	24
Figure 3.3: Laser Slots on Workpiece	24
Figure 3.4: CNC Micro Milling Machine with Ultrasonic Setup.....	25
Figure 3.5: Ultrasonic Setup along with the Work Piece and Cutting Tool	26
Figure 3.6: Setup of Olympus Digital Microscope to Measure Response Values	27
Figure 3.7: Magnified Images for Surface Roughness, Tool Wear and Burr Formation	28
Figure 3.8: Details of Work Methodology.....	30
Figure 4.1: All Sixteen Slots Showing Surface Roughness.....	31
Figure 4.2: Main Effect Plots for Means and S/N Ratios of Surface Roughness	33
Figure 4.3: Tool Wear in All Sixteen Experiments	34
Figure 4.4: Main Effect Plots for Means and S/N Ratios of Tool Wear.....	36
Figure 4.5: Burr Formation in All Experimental Runs	37
Figure 4.6: Main Effect Plots for Means (a, b, c and d) and Main Effect Plots for S/N Ratios (e, f, g and h) of BWDM, BHDM, BWUM and BHUM	42
Figure 4.7: Collective Main Effect Plots of Means and S/N Ratios of BWDM, BHDM, BWUM and BHUM.....	43
Figure 5.1: Main Effect Plots for S/N Ratios of (a) Surface Roughness, (2) Tool Wear, (3) Burr in Down Milling and (4) Burr in Up Milling.....	46
Figure 5.2: Response Surface Regression of W-GRG (a) Histogram; (b) Pareto Chart; (c) Normal Probability Plot for Residual; (d) Observation Order of Residual	53
Figure 5.3: Graph of Multiple Response Prediction	54
Figure 5.4: Workpiece After RSM-Optimized Run.....	54

List of Tables

Table 3.1: Chemical Composition of Inconel 718	22
Table 3.2: Specification Details of Tools.....	23
Table 3.3: Details of Laser Marking Machine	24
Table 3.4: Depth of Laser Slots	25
Table 3.5: Experimental Conditions [12].....	26
Table 3.6: Selected Parameters and their Levels	27
Table 3.7: Average Response Values Along with Their Cutting Parameters	29
Table 4.1: Analysis of Variance for Surface Roughness	32
Table 4.2: Response Table for Means of Surface Roughness.....	32
Table 4.3: Response Table for S/N Ratios of Surface Roughness.....	33
Table 4.4: Analysis of Variance for Tool Wear.....	35
Table 4.5: Response Table for Means of Tool Wear	35
Table 4.6: Response Table for S/N Ratios of Tool Wear	35
Table 4.7: Analysis of Variance for BWDM	37
Table 4.8: Analysis of Variance for BHDM	38
Table 4.9: Analysis of Variance for BWUM	38
Table 4.10: Analysis of Variance for BHUM	38
Table 4.11: Response Table for Means of BWDM	39
Table 4.112: Response Table for S/N Ratios of BWDM.....	39
Table 4.13: Response Table for Means of BHDM	39
Table 4.114: Response Table for S/N Ratios of BHDM.....	39
Table 4.15: Response Table for Means of BWUM	40
Table 4.116: Response Table for S/N Ratios of BWUM.....	40
Table 4.17: Response Table for Means of BHUM	40
Table 4.18: Response Table for S/N Ratios of BHUM	40
Table 4.119: Response Table for Collective Means of BWDM, BHDM, BWUM and BHUM	41
Table 4.20: Response Table for Collective S/N Ratios of BWDM, BHDM, BWUM and BHUM.....	41

Table 4.21: Average S/N Ratios for Surface Roughness (SR), Tool Wear (TW), Burr Formation in Down Milling (BDM) and Burr Formation in Up Milling	44
Table 5.1: Data Grey Relational Generation and Deviation Sequence.....	48
Table 5.2: Eigenvector Representing Weights for All Response Variables	48
Table 5.3: GRC and W-GRG Values for All Response Variables	50
Table 5.4: Response Table for Means of W-GRG.....	50
Table 5.5: Analysis of Variance for W-GRG	51
Table 5.6: Regression Equations for W-GRG (speed, FR, DoC, and Amp) with Different TCs	52
Table 5.7: Multiple Response Prediction Along with Their Parameters	53
Table 5.8: Comparison of Best Run and RSM Optimized Run	54

CHAPTER 1: INTRODUCTION

Due to the numerous applications that micro-components can be seen in, particularly in the aerospace, automobile, electronics, and green energy sectors as well as the biomedical sciences, micromachining has garnered a lot of attention recently. [1]. These tiny systems or products are usually built from materials such as composites, metal alloys, polymers, and ceramics. These materials exhibit intricate shapes and are challenging to machine. [2]. The accuracy of micro-features like microchannels, micro-holes, and micro-pockets, among others, is essential to the performance of micro-components. [3]. For example, a vital role is played by accuracy of microchannels in biomedical settings, including microfluid systems [4]. For a precise machining of such intricate-shaped and tiny-scaled components, very accurate tools and machinery is required. A comparison of different micro and nano-scaled material removal techniques [5-11], is depicted in Figure 1.1. Numerous researchers have shown interest in macro machining for the last couple of decades, but evolving towards micro sector is not as simple as scaling down macro domain features. Therefore, perceiving the technical aspects of micro machining require more distant research [12].

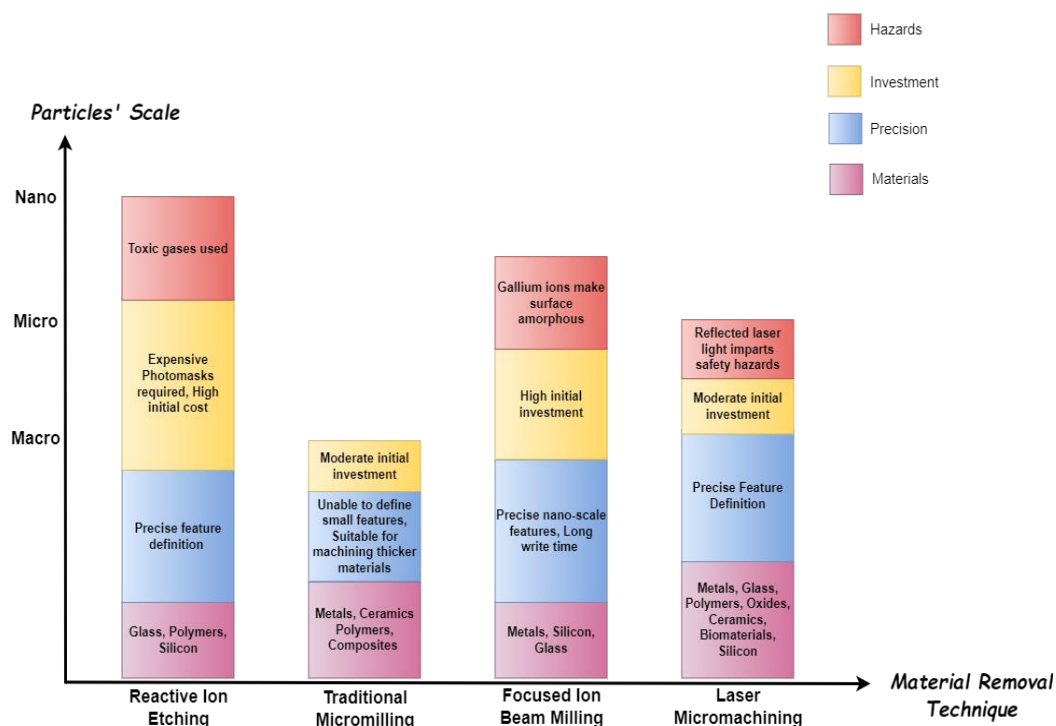


Figure 1.1: Comparison of Different Material Removal Techniques

In situations where there is a lot of heat, corrosion, and stress, such as in aerial engines for gas turbines, working conditions are very complex and challenging. Such conditions

vigorously demand high-resisting and high-performance super alloys [13-16]. For instance, in Figure 1.2, steel is compared with super alloys on the basis of their yield strengths at high temperature. Heat-resistant super alloys based on nickel, such Inconel 718, provide exceptional mechanical characteristics at temperatures as high as 700 °C [17], and are frequently used in the production of parts for airplane, rocket, and submarine systems whose ambient temperature ranges from 450 °C to 700 °C [18, 19]. Unluckily, the features that make it one of the most demanding engineering materials are also contributing to its inadequate machining, which typically leads to excessive tool wear and subpar surface quality, both of which raise the product's price. [20-22]. These are the primary factors that draw in a large number of researchers to carry out different investigations meant to maximize the machinability of this kind of material.

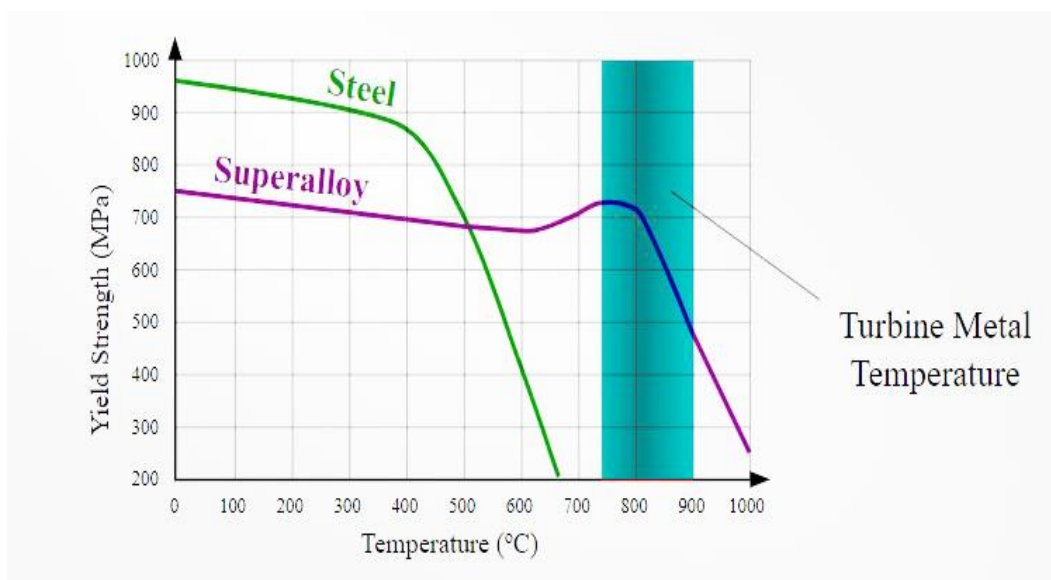


Figure 1.2: Comparison of Superalloys with Steel at High Temperature Environments

1.1 Research Motivation

Micro machining is vital for extensive research and development in many fields, as it plays a crucial role in working with advanced materials. Such materials are proven to be very difficult for delicate machining [2]. For micro machining of such materials, we need to find out such optimal cutting parameters which can result in better surface quality, lower tool wear and reduced burr formation. From literature, it is evident that many hybrid processes are able to machine superalloys with desirable results; including ultrasonic assisted micro milling and

laser embedded ultrasonic milling [23, 24]. So, Laser-based ultrasonic assisted low speed micro milling (LLUMM) is suitable for micro-milling of hard-to-machine materials like Inconel-718.

One of the primary challenges with mechanical machining is burr formation. Whether macro machining or micro machining, unwanted burrs are produced in both cases. In macro machining, deburring is not that difficult due to larger burr size, but micro machining produces minute burrs which complicates the deburring operation. It can deteriorate the workpiece as well as delicate micro features in micro components [25]. Also, deburring necessitates assembly procedures which makes it an expensive extra operation; therefore, it is highly undesirable operation for reducing burrs [26]. For reducing burr formation, AJ Mian improved the cutting conditions for the micro-milling process of Inconel-718 with uncoated and AlTiN coated tools with a 0.5 mm diameter [27], yet, the impact of varying cutting speeds on burr development is not clearly mentioned in his research. Most of the literature suggests high cutting speeds for efficient micro machining, therefore, the effects of low cutting speeds need more investigation. Also, low speed milling setups are cost-effective and quite attainable as compared to high-speed milling setups. Therefore, this study focuses on low speed (conventional machining range) for observing multi-factor effect on output responses.

1.2 Research Objectives

- To enhance the material removal rates through laser-based ultrasonic machining of superalloys
- To explore low-speed machining of superalloys by employing laser-based ultrasonic
- To highlight the machining complexities during the laser-based ultrasonic machining
- To inquire about the structural attributes like burr creation, tool wear, and roughness of the surface, resulted from LLUMM.
- Using multiple optimization techniques to enhance the quality of surfaces during machining, lower tool wear, and reduced burr formation.

1.3 Research Scope

This study project is confined to the LLUMM of Inconel-718 with constant depth (20 micron) of laser-slots. It utilizes both uncoated and TiAlN, TiSiN and nACo coated tools with 0.5 mm diameter carbide end-mill working under the tool speed of 6-11 m/min speed and below 8000 rpm. Low speed machining is selected because of its cost-effectiveness and easy

accessibility. The prime focus of the study is to observe burr creation, tool wear, and roughness of the surface under prescribed conditions.

1.4 Areas of Application

Lasers-based ultrasonic machining has several applications in the manufacturing sector, including welding, cladding, marking, surface treatment, drilling, and cutting. Precision machining of complex parts is essential in many fields, including aerospace engineering, vehicle manufacturing, shipbuilding, electronics, and even medicine. When compared to conventional metals, superalloys excel in several key areas: durability, surface stability, corrosion resistance, and mechanical strength [28]. This makes them ideal for use inside the aviation industry, in the fabrication of engines for turbine and other high-stress industrial applications. Used widely in aero-planes, factories, rockets, spaceships, nuclear power plants, submarines, electric motors, chemical storage tanks, heat exchanger pipes, and many more applications.

CHAPTER 2: LITERATURE REVIEW

The necessity of new materials and assembly methods increases over time, and innovations are on track. As we endeavour to manufacture small and compact parts, advancements in technology are also pushing us towards the need for miniature machine parts, forcing us to offer standard solutions to complex problems. Presently, standard machining methods up to micro-machining has been established to address the requirements of miniature parts and have many advantages over traditional machining methods. Figure 2.1 depicts the machining accuracy of different machining technologies over time [29]. Ultrasonic, laser, electro discharge, and electro-chemical assisted machining are at the forefront of the effort, with a focus on enhancing the machinability of nickel-based superalloys and metal matrix composite (MMC) materials; two types of aerospace alloys that have historically proven challenging to machine [30].

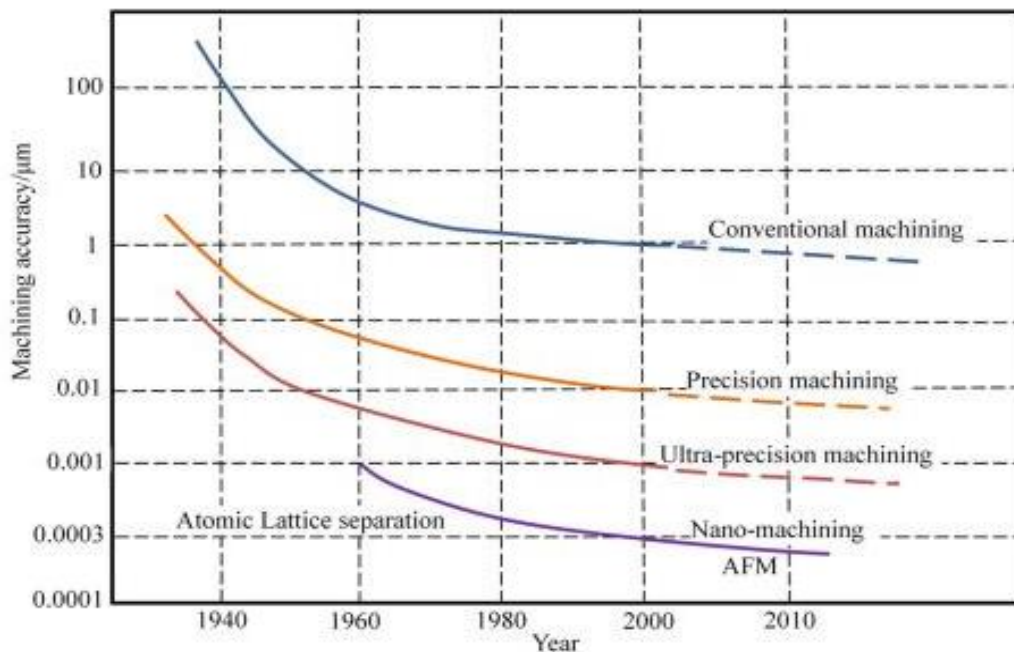


Figure 2.1: Machining Accuracy of Different Machining Techniques Over Time

Despite their usefulness as components in aircraft and medical implant technologies because to their excellent ratio of strength to weight, super alloys have a poor reputation for being difficult-to- make because of their unusual thermomechanical properties. Many investigations have focused on the feasibility of employing various energy field machining techniques to improve the machinability of these alloys [31]. By producing high-frequency

vibrations in one or more cutting directions, ultrasonic-assisted machining (UAM) improves the machinability of high-strength alloys by causing cyclic loads and unloads on the tool used for cutting. Various tests have shown that laser-assisted ultrasonic machining (LUM) can increase machinability by locally heating the workpiece at the cutting edge [32]. This allows for clean cuts to be made with little effort.

Because nickel-based superalloys like Inconel-718 are difficult to mill, the best possible combination of machining parameters is needed to provide improved surface quality, less tool wear, and decreased burr development. Numerous academics have looked into the factors influencing surface roughness during cutting of such materials, in an effort to optimize such parameters [33-38]. It has been demonstrated that multiple factors, including cutting speed, feed rate, tool diameter, and type of tool coatings, significantly affect surface roughness. Another response variable that has drawn the attention of researchers is tool wear. The literature has confirmed that tool wear is a significant issue when machining Inconel-718. [39]. Cutting speeds at all levels are hugely responsible for tool wear [40] but the tool life can be enhanced by using Titanium Aluminium Nitride (TiAlN) coating [41]. Although, numerous tasks have been completed on process optimization of Inconel-718 machining, low speed micro processing of such alloys still requires an extensive study for its micro features [12].

2.1 Hybrid Micro Machining

In order to produce miniature and micro-scaled components with great precision and accuracy, hybrid micro machining techniques combine two or more machining processes. Figure 2.2 depicts different types of hybrid micro machining techniques [24].

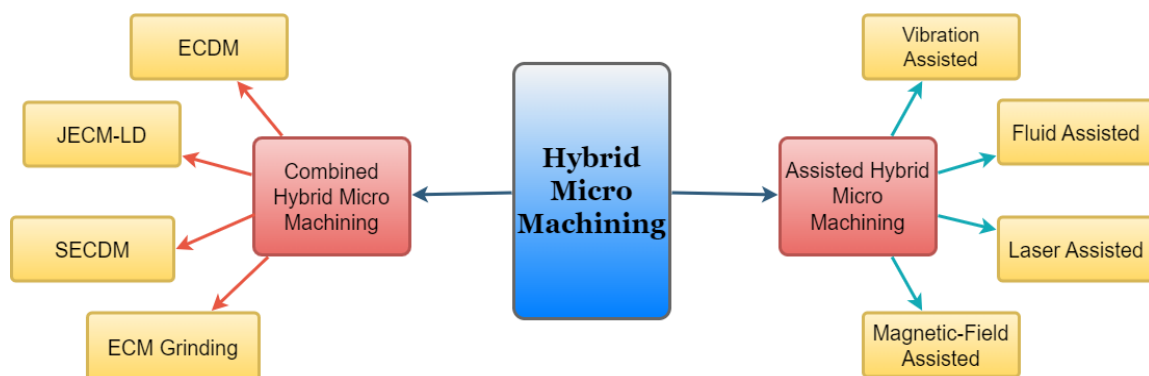


Figure 2.2: Classification of Hybrid Micro Machining Techniques

2.2 Laser-Based Ultrasonic Assisted Low Speed Micro Milling (LLUMM)

LLUMM represents a kind of hybrid machining where vibration assisted (ultrasonic) and laser assisted hybrid techniques are combined. LLUMM gets the benefits of Laser Beam Machining (LBM) including versatile machining of complex shapes, no tool wear, removal of material without contact, and simple and cost-effective micro machining etc. LBM uses a high-power laser pulse at a particular point of workpiece to subtract material from that point. The feasibility of LBM in producing micro components has been studied for many material including polymers [42-45], glass [46-48], alloys [49-51], metals [52, 53], and ceramics [54-58]. LLUMM also takes the advantages of Ultrasonic Machining (USM) including precision and accuracy, variability and flexibility, no heat-affected zones, lesser tool wear and environmentally friendly machining etc.

High frequency electrical signals are sent to a transducer in USM, where they are transformed into mechanical vibrations. These vibrations are captured by an energy-focusing device (horn/tool assembly), which uses them to create high-frequency vibrations (typically ≥ 20 kHz) along the tool's longitudinal axis. The tool vibrates in the axis of tool feed to remove material from the workpiece [59]. This technique has been employed in numerous works for micro machining of various alloys including nickel and titanium alloys [60].

Literature is evident that LBM and USM has been carried out for a variety of materials. But there is little information regarding study of vibration and/or laser assisted micromachining of Inconel-718, especially for optimizing multi factors simultaneously. Using various degrees of multiple factors, such as cutting speed, feed rate, depth of cut, and vibration amplitude for both coated and uncoated tools, this study will employ LLUMM to optimize surface roughness, tool wear, and burr creation simultaneously.

CHAPTER 3: EXPERIMENTAL SETUP

3.1 Work Piece Material

In this work, milling tests were conducted on a sample of 10 mm thick Inconel 718 that had 50 mm of length and 10 mm of breadth. Inconel 718 is noted for having outstanding weldability because of its comparatively slow precipitation kinetics. It also has strong strength, long fatigue life, and creep resistance at increased temperatures up to 700°C. [61, 62]. It is a precipitation-hardened niobium-modified nickel-iron alloy with the nominal composition shown in Table 3.1 [63, 64].

Table 3.1: The Chemical Constitution of Inconel 718

Element	Ni	Cr	Fe	Nb	Mo	Ti
Weight by %	54.59	19.16	17.47	4.85	2.88	1.05

The work piece was first grounded and polished, then treated with waterless Kaling's Chemical for about 5 seconds before being cleansed with water. A Vickers Micro Hardness Tester was used to measure the hardness on Vickers scale for the work piece, which was discovered to be 361 HV. A 9800 Nm force and a 6 s dwell period were used for the hardness tests.

3.2 Cutting Tools and Conditions

Electric Discharge Machining (EDM) was used to create the work piece, having 10 x 50 x 50 mm dimensions. A 10 mm cutting length was set for each slot to perform test, while each slot was spaced 1.5 mm apart from the other, as shown in Figure 3.1.

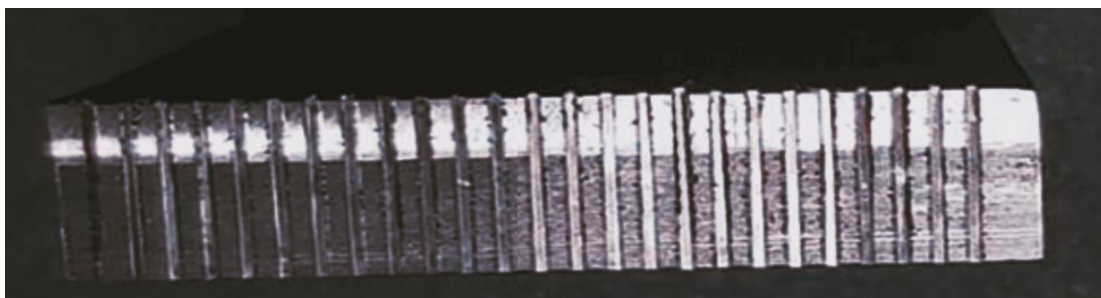


Figure 3.1: Machined Slots on Inconel 718

Four types of different Tungsten Carbide Flat End Mill cutting tools were used for micro milling. One of the tool types was uncoated, while others having coating of Titanium Aluminium Nitride (TiAlN), Titanium Silicon nitride (TiSiN), and Aluminium Titanium Nitride + Silicon Nitride (nAlCo) as shown in Figure 3.2. Here are some further details on the tools in Table 3.2.

Table 3.2: Details of the Tools' Specifications

Detail	Information
Brand Name	Changzhou North Carbide Tool Co
Material	Tungsten Carbide Steel
Type	End mill
Number of Flutes	02
Diameter(mm)	0.5
Overall Length(mm)	50
Rockwell hardness (HRC)	60
Cobalt Content (%)	12
Balde Length(mm)	1
Helix Angle	35
Grain Size	0.5
Flexural Length	4300

3.3 Split Type Lase Marking Machine

Prior to micro milling, pre-slots were made by laser cutting to increase the process's overall efficiency, as laser machining offers a high productivity [65]. A split type laser marking machine of TS-20F type was used for the purpose. Further details of the laser machine are given in Table 3.3.

Table 3.3: Details of Laser Marking Machine

Details	Specifications
Type	TS-20F
Power	20W
Laser Brand	Maxphotonics (Raycus/IPG Optional)
Marking Area	110mm*100mm
Marking Depth (max.)	0.5mm
Marking Speed (max.)	7000mm/s
Focus Spot Diameter	<0.01mm
Output Power of Laser	10% to 100% (continuously to be adjusted)

A ‘hit and trial’ method was applied to adjust the laser cutting parameters for making the pre-slots of $20\pm 1 \mu\text{m}$. The parameters were fixed at Loop Count = 120, Speed = 100 mm/s, Power % = 80, and Frequency (KHz) = 20. ‘Laser machine setup’ and ‘work piece with laser slots’ is depicted in Figure 3.2 and Figure 3.3 respectively.

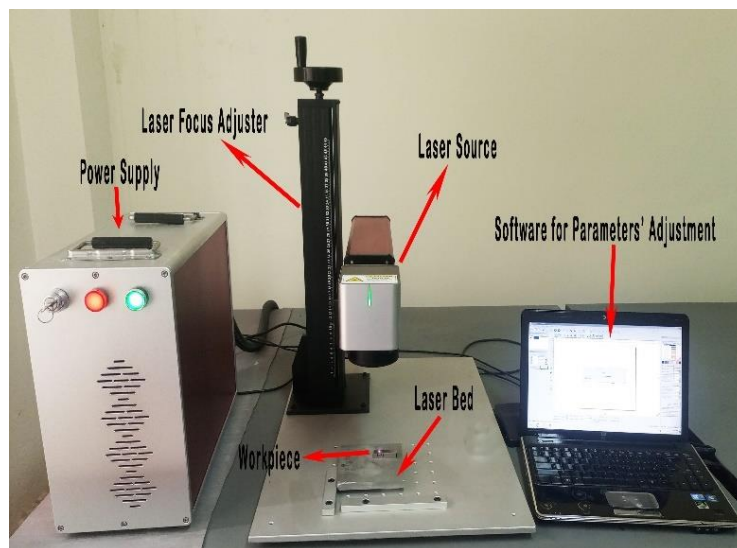


Figure 3.2: Setup of Laser Machine

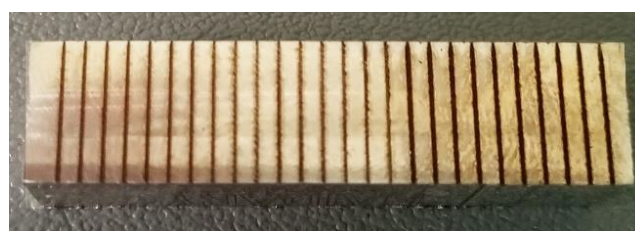


Figure 3.3: Laser Slots on Workpiece

The depth of cut of 16 laser slots were measured with DSX programming, using Olympus Digital Microscope. Table 3.4 depicts the depth of each laser cut.

Table 3.4: Depth of Laser Slots

Slot No.	1	2	3	4	5	6	7	8	9	10	11	12	13	14	15	16
Depth (μm)	20.0	20.4	19.7	20.3	20.0	20.8	19.4	19.6	19.9	20.0	19.5	19.6	20.0	20.7	20.1	20.0

3.4 CNC Milling Machine with Ultrasonic Setup

After laser slotting, the pre-slots were machined on CNC milling machine for the required depths. The micro milling process was carried out using a FANUCMV-1060 standard speed machining focus, as presented in Figure 3.4.



Figure 3.4: CNC Micro-Milling Machine with Ultrasonic Setup

During the micro milling process, a FANUC 0i-MC Movement Regulator controlled the whole motion of the workpiece in relation to the cutting tool. Levelling of the work piece's surface was initially carried out using a presetting device. A device pre setter was installed in the z-pivot for making precise predictions. The device was subjected to 1D vibrations using a 3-kW piezoelectric transducer, an MPI ultrasonic generator, and high-recurrence electrical stimulation from a 50 KHz electrical source (ACROW MACHINERY MANUFACTURING COMPANY LTD TAIWAN). Those high frequency and high pulse beats were transformed

into ultrasonic mechanical vibrations (23 kHz) after entering the transducer. The whole ultrasonic setup is represented in Figure 3.5.

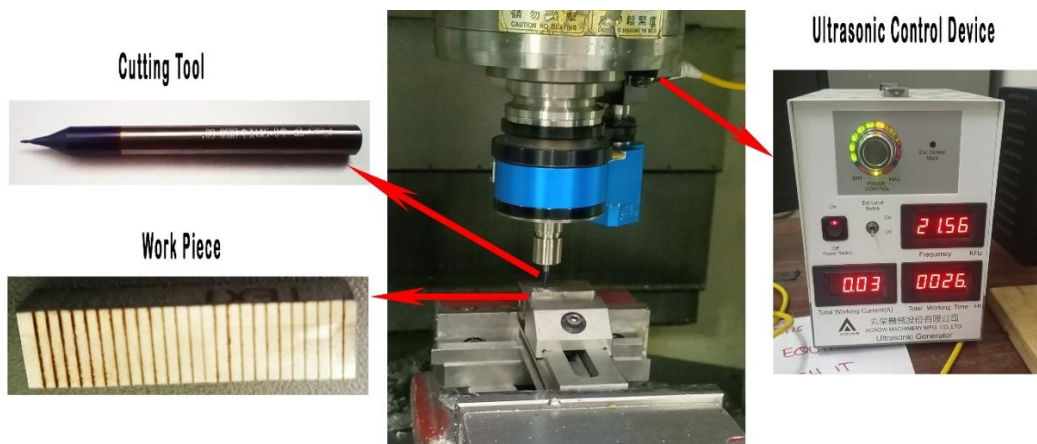


Figure 3.5: Cutting Tool and Workpiece Along with the Ultrasonic Setup

All the experiments were carried out under certain conditions, shown in Table 3.5.

Table 3.5: Conditions for Experiments [12]

Work Piece Material	Inconel-718
Diameter of the Tool	0.5 mm
Flute Numbers	02
Length of Cut	10 mm
Conditions for Cutting	Dry
Type of Milling	Full Immersion

3.5 Selection Parameters for Cutting

This research assessed several tool coatings in addition to four machining parameters: feed rate, depth of cut, amount of hardware vibration, and spindle speed. These parameters' ranges and values were selected in accordance with the literature. [12, 66], referring to ISO principles and tool manufacturing guidelines. Table 3.6 shows every parameter that has been chosen, along with each one's level.

Table 3.6: Selected Parameters and their Levels

Parameters	Level 1	Level 2	Level 3	Level 4
Speed (m/min)	6	7.5	9	10.5
Feed ($\mu\text{m}/\text{tooth}$)	0.25	0.5	0.75	1.0
Depth of Cut (μm)	30	50	70	90
Coating	Uncoated	TiAlN	TiSiN	nACo
Amplitude	0	3	6	9

3.6 Response Variables

This research is focused to estimate four responses; Surface Roughness (SR), Tool Wear (TW), Burr Formation in Up Processing (BUM), and Burr Formation in Down Processing (BDM). The response variables were estimated by utilizing DSX amplification programming. The surface foulness of each space was estimated by using a DSX Olympus Digital magnifying lens as shown in Figure 3.6, which empowered the recognizable proof of miniature surfaces in processing tasks. The surface foulness and the tool wear were evaluated in microns, by utilizing the ISO 4287 and ISO 8688-1/ISO 8688- 2 standards respectively [67-69].

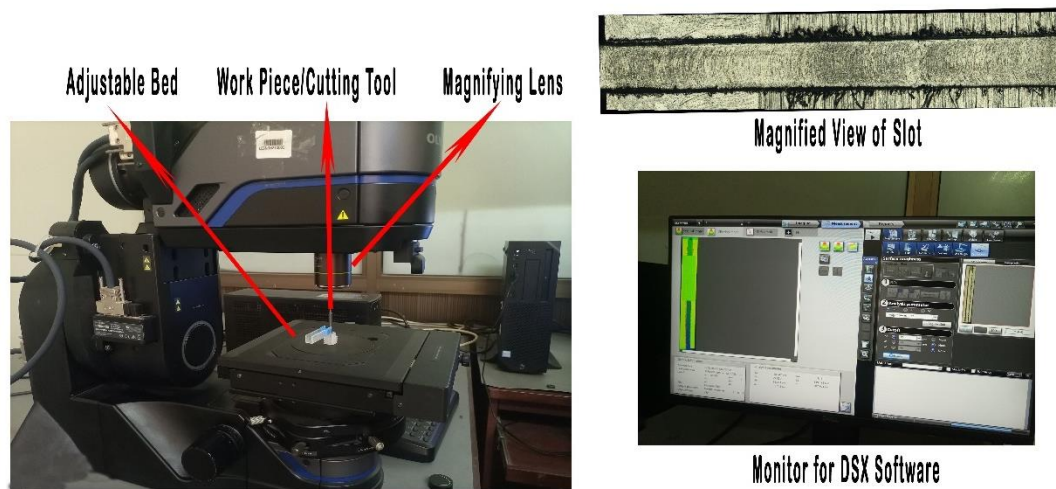


Figure 3.6: Setup of Olympus Digital Microscope to Measure Response Values

All the response variables are briefly defined in the following:

Surface Roughness; Regardless of how they are formed, solid surfaces exhibit irregularities or deviations from the specified geometric shape [70-73]. Those irregularities or deviations are known as surface roughness, which can be of different magnitudes, ranging from shape deviations to irregularities on the order of interatomic distances.

Tool Wear; Tool wear is, when a tool changes its shape during cutting operations and deviates from its original shape due to the gradual loss of material. Corrosion, fracture, abrasion, erosion, diffusive wear and material adhesion are some the reasons for tool wear [74-76].

Burr Formation; According to ISO 13715 [77], burr is formed when the overhang of a workpiece's edge exceeds zero value. Flash or burr is that part of a workpiece that is created as an unwanted geometry on an edge or a surface during the manufacture of a product. Ko defines flash as an unwanted material protrusion created by plastic flow during a cutting or shearing operation [78]. According to Gillespie, burrs fall within the theoretical intersection and are limited to cutting and shearing operations [79].

SR, TW and Burr Formation are shown in Figure 3.7.

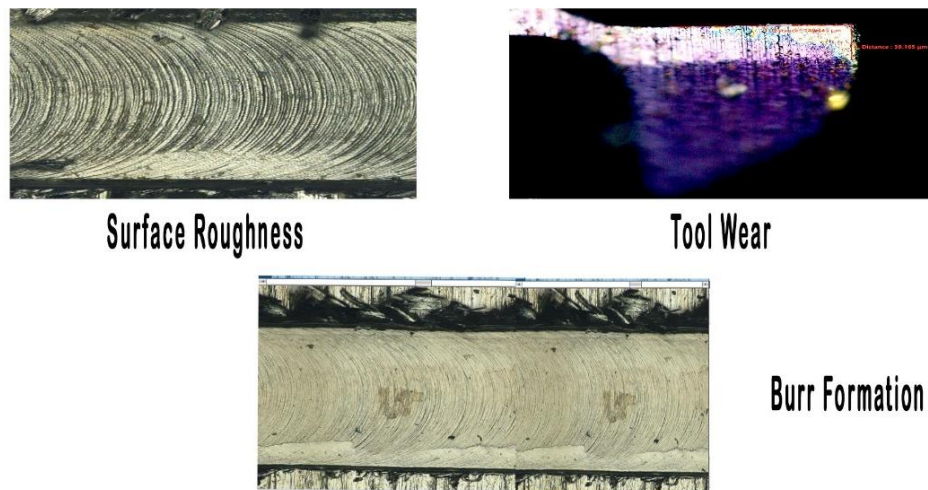


Figure 3.7: Magnified Images for SR, TW and Burr Formation

3.7 Design of Experiments

This research work employed Taguchi orthogonal arrays to obtain a design matrix that involved a limited number of experiments and covered the entire parametric space. Although optimization of various engineering problems is carried out by using Taguchi method, but it is limited to mono- optimization processes [80-82]. When a problem requires optimization of multiple responses, this method lacks its efficiency [83]. Multi-objective optimization techniques are used in such cases, as Grey Relational Analysis (GRA) embedded with Principal Component Analysis (PCA) [84] is employed in this work.

To effectively use the responses of fewer runs, Taguchi design of experiments was used to develop an orthogonal L16 array [85-87] for sixteen experiments. Many researchers have successfully employed Taguchi arrays for definitive findings in the past, for various factors at different levels [67, 88-90]. Each experimental run was repeated twice for measuring responses two times each. Table 3.7 depicts average values of all the measured responses, along with their machining parameters. To determine the separate and cumulative impacts of the machining parameters on the responses, all the data was statistically evaluated.

Table 3.7: Average Response Values Along with Their Cutting Parameters

Exp. #	Speed (m/min)	Feed ($\mu\text{m}/\text{tooth}$)	Depth of Cut (μm)	Tool Coating	Amplitude (μm)	Tool Wear (μm)	Surface Roughness (μm)	Burr Width Down Milling (μm)	Burr Height Down Milling (μm)	Burr Width Up Milling (μm)	Burr Height Up Milling (μm)
1	6	0.25	30	Uncoated	0	31.226	0.065	127.159	149.361	109.440	42.36
2	6	0.5	50	TiAlN	3	32.431	0.071	147.177	153.627	114.363	50.591
3	6	0.75	70	TiSiN	6	29.65	0.057	159.24	134.571	145.540	76.583
4	6	1	90	nACo	9	31.819	0.051	163.113	147.32	175.496	81.233
5	7.5	0.25	50	TiSiN	9	27.625	0.045	161.225	155.735	132.129	29.751
6	7.5	0.5	30	nACo	6	31.591	0.059	169.2	149.048	83.250	26.8
7	7.5	0.75	90	Uncoated	3	36.021	0.063	159.161	201.4	160.600	88.526
8	7.5	1	70	TiAlN	0	36.1	0.101	181.288	185.726	157.281	91.912
9	9	0.25	70	nACo	3	37.124	0.031	194.284	178.45	148.912	64.637
10	9	0.5	90	TiSiN	0	34.217	0.038	199.157	184.182	159.007	87.504
11	9	0.75	30	TiAlN	9	34.731	0.058	165.203	155.29	158.836	61.461
12	9	1	50	Uncoated	6	34.043	0.051	171.22	171.364	175.680	93.128
13	10.5	0.25	90	TiAlN	6	35.42	0.045	214.18	191.754	167.045	91.802
14	10.5	0.5	70	Uncoated	9	33.391	0.034	203.307	197.208	170.490	71.288
15	10.5	0.75	50	nACo	0	37.829	0.061	166.244	186.27	148.362	103.389
16	10.5	1	30	TiSiN	3	36.502	0.062	158.226	168.466	153.924	78.308

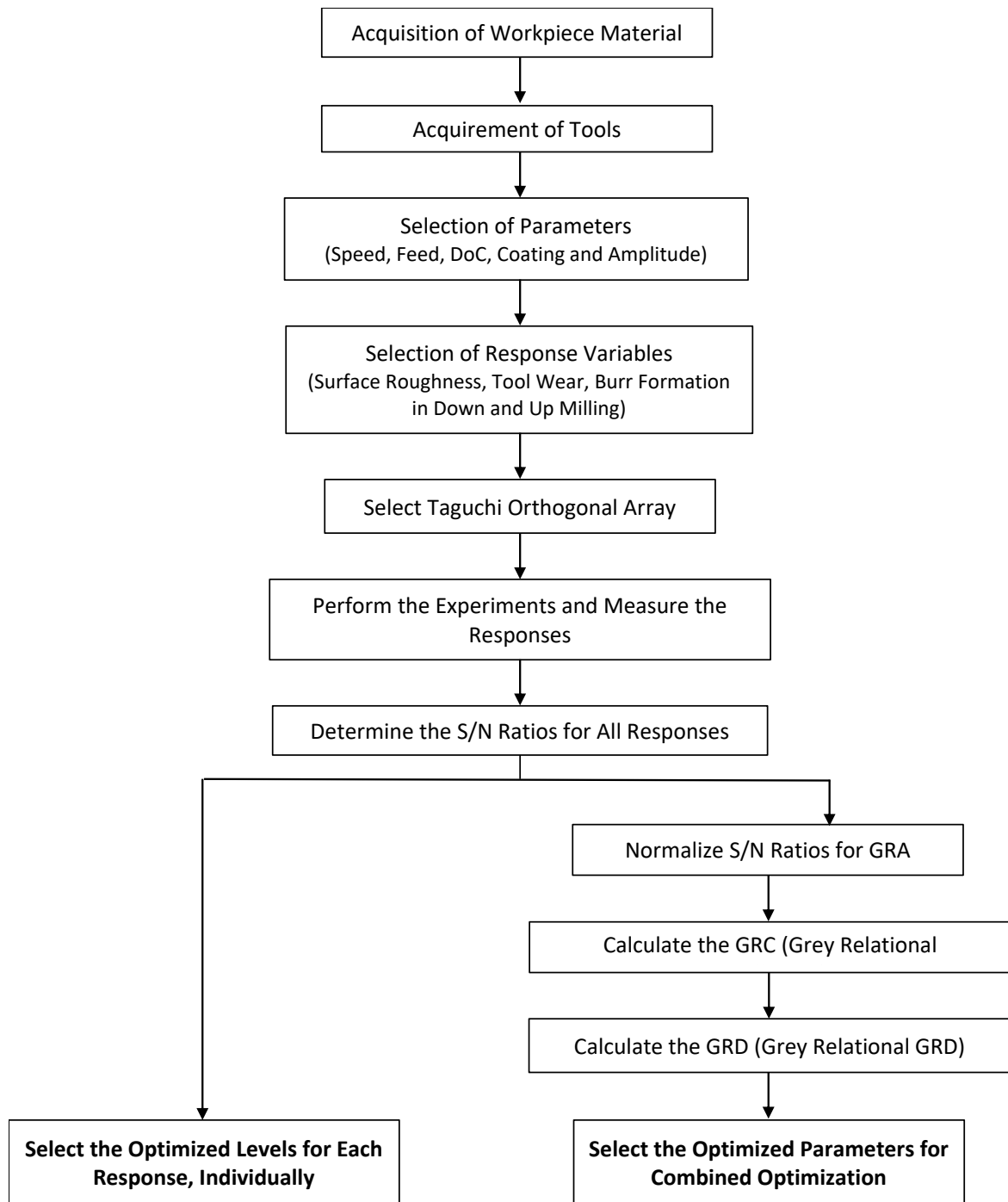


Figure 3.8: Details of Work Methodology

CHAPTER 4: OPTIMIZATION OF INDIVIDUAL RESPONSES

4.1 Analysis of Variance

A statistical technique called analysis of variance (ANOVA) examines the means of several samples [91]. In order to maximize each outcome independently, ANOVA was used in this investigation. The base for ANOVA hypothesis test is to compare two independent variables of population variance [92]. The following postulations are compulsory for performing ANOVA successfully:

- There is independence of variables on each another
- Each group's observations are normally distributed
- The variance in population is same for all groups

4.2 Surface Roughness

Many elements, such as vertical step size, feed rate, tool diameter, spindle speed, depth of cut, tool coating, and ultrasonic excitation of the tool head, have a substantial impact on how rough a metal surface is. [93-97]. In Figure 4.1, parts of all the sixteen experimental slots are shown.

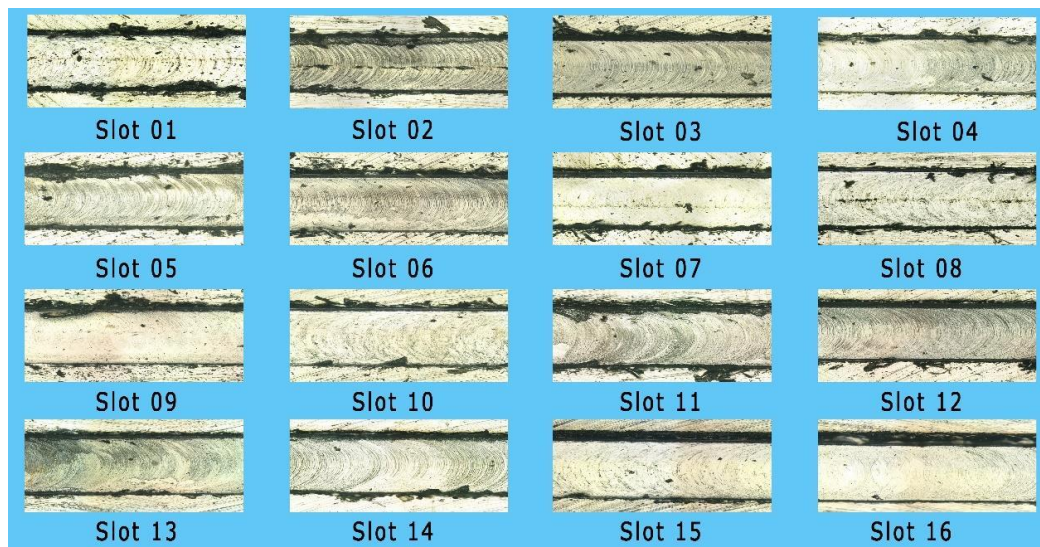


Figure 4.1: All Sixteen Slots Showing Surface Roughness

ANOVA was performed for the experimental data to check and optimize the effects of selected factors (Speed, Feed, DoC, Coating and Amplitude) on roughness of slot's surfaces. Table 4.1 represents the results of this analysis.

Table 4.1: Analysis of Variance for Surface Roughness

Source	DF	Seq SS	Contribution	Adj SS	Adj MS	F-Value	P-Value
Regression	7	0.003474	82.77%	0.003474	0.000496	5.49	0.014
Speed	1	0.000586	13.96%	0.000586	0.000586	6.48	0.034
FR	1	0.000942	22.44%	0.000942	0.000942	10.42	0.012
DoC	1	0.000272	6.48%	0.000272	0.000272	3.01	0.121
Amp	1	0.000747	17.80%	0.000747	0.000747	8.27	0.021
TC	3	0.000927	22.08%	0.000309	0.000309	3.42	0.073
Error	8	0.000723	17.23%	0.000090	0.000090		
Total	15	0.004197	100%				

In order to get the answers for the Signal to Noise (S/N) Ratio and Data Means, the data was further examined using Taguchi Analysis. The 'smaller is better' approach was used for the S/N ratio since the objective was to reduce surface roughness. The smaller, the better S/N ratio is computed by Equation (1):

$$S/N \text{ ratio} = -10 \times \log_{10} \left\{ \frac{\sum (Y)^2}{n} \right\} \quad (1)$$

where n is the number of replications and Y is the measured observation.

Response tables for means and S/N ratios are shown as Table 4.2 and Table 4.3, while Figure 4.2 graphically represents the data of these tables.

Table 4.2: Response Table for Means of Surface Roughness

Level	Speed	FR	DoC	TC	Amp
1	0.06100	0.04650	0.06100	0.05325	0.06613
2	0.06700	0.05038	0.05700	0.06875	0.05675
3	0.04437	0.05975	0.05575	0.05038	0.05300
4	0.05050	0.06625	0.04913	0.05050	0.04700
Delta	0.02263	0.01975	0.01187	0.01837	0.01913
Rank	1	2	5	4	3

Table 4.3: Response Table for S/N Ratios of Surface Roughness

Smaller is better

Level	Speed	FR	DoC	TC	Amp
1	24.36	26.95	24.30	25.74	24.12
2	23.86	26.36	25.01	23.64	25.33
3	27.32	24.48	26.08	26.12	25.56
4	26.19	23.94	26.33	26.22	26.72
Delta	3.46	3.01	2.03	2.59	2.60
Rank	1	2	5	4	3

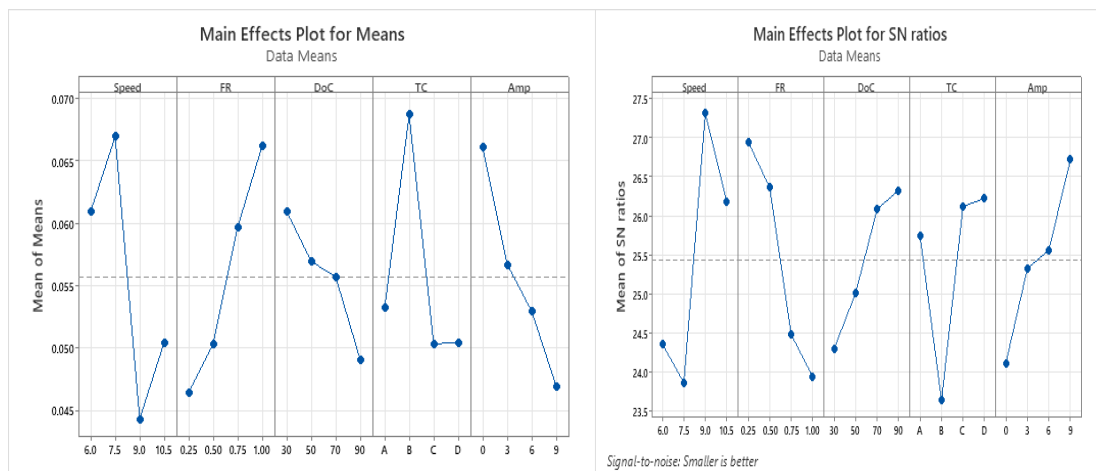


Figure 4.2: Main Effect Plots for Means and S/N Ratios of Surface Roughness

It is clear from the statistical study above, that each element influences surface roughness to some degree. In relation to the impact on surface roughness, the following elements are ordered in descending order as speed, feed rate, amplitude, tool coating and depth of cut. The following inferences are drawn from the aforementioned graphs:

- Cutting speed is the dominant factor to affect surface quality. It affects the roughness at lower speeds significantly, but improves at higher speed because of the thermal softening effect.
- In case of the feed rate, it directly affects the surface quality as; lower the feed rate, lower is the surface roughness. At higher feed rates, thicker chips are removed from the workpiece surface which leads to potential surface irregularities.
- At lower amplitude, surface quality is compromised. But as the amplitude increases, it notably improves the surface quality. Higher amplitudes prevent excessive dwell time, promotes more efficient material removal and reduce average cutting forces along with cracks propagation [98-100]. This can result in reducing potential for work hardening effects, leading to improved surface finish.

- Surface roughness is higher at lower depth and decreases as the depth increase. This is because of the roughness and cracks due to laser pre-slotting. For tool coatings, brittle materials are easily worn as compared to the ductile materials. Less worn-out tool results in better surface quality, as in case of TiAlN.

4.3 Tool Wear

Surface quality, dimensional accuracy, and tool life are just a few of the machining processes that can be significantly impacted by tool wear. The most prevalent type of tool wear is called flank wear, and it significantly affects surface roughness. It is caused by continuous frictional forces between the cutting tool's flank (side) and the workpiece material. [89]. The tool wear in all experiments is shown in Figure 4.3.

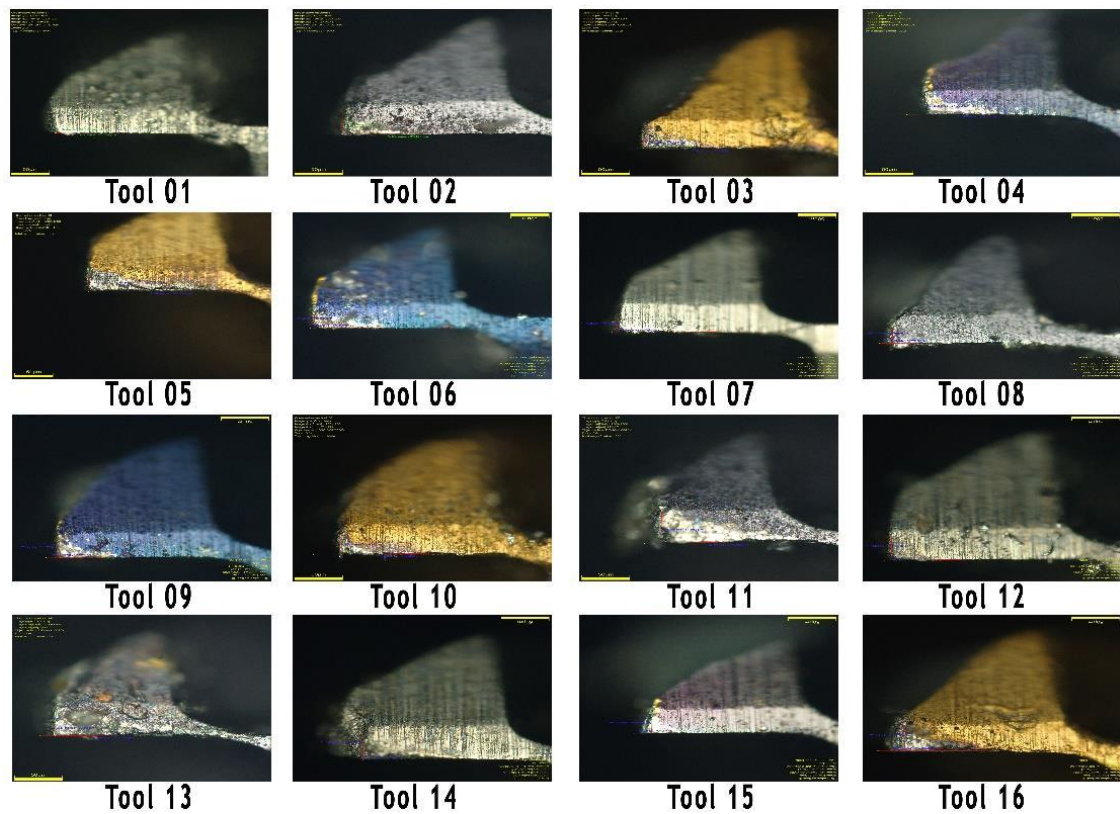


Figure 4.3: Tool Wear in All Sixteen Experiments

The experimental data underwent ANOVA analysis, and the outcomes regarding the influence of each component on tool wear are illustrated in Table 4.4.

Table 4.4: Analysis of Variance for Tool Wear

Source	DF	Seq SS	Contribution	Adj SS	Adj MS	F-Value	P-Value
Regression	7	107.553	88.68%	107.553	15.365	8.95	0.003
Speed	1	49.339	40.68%	49.339	49.339	28.75	0.001
FR	1	9.666	7.97%	9.666	9.666	5.63	0.045
DoC	1	2.671	2.20%	2.671	2.671	1.56	0.247
Amp	1	27.369	22.57%	27.369	27.369	15.95	0.004
TC	3	18.508	15.26%	18.508	6.169	3.60	0.066
Error	8	13.728	11.32%	13.728	1.716		
Total	15	121.281	100%				

By further analyzing the results using Taguchi Analysis, responses for S/N Ratios and Data Means were calculated. Again, for S/N ratio, 'smaller is the better' approach was preferred to minimize tool wear. Table 4.5 and Table 4.6 represent Main Effect Plots for means and S/N ratios respectively while the data of these tables is graphically shown in Figure 4.4.

Table 4.5: Response Table for Means of Tool Wear

Level	Speed	FR	DoC	TC	Amp
1	31.28	32.85	33.51	33.67	34.84
2	32.83	32.91	32.98	34.67	35.52
3	35.03	34.56	34.07	32.00	32.68
4	35.79	34.62	34.37	34.59	31.89
Delta	4.50	1.77	1.39	2.67	3.63
Rank	1	4	5	3	2

Table 4.6: Response Table for S/N Ratios of Tool Wear

Smaller is better

Level	Speed	FR	DoC	TC	Amp
1	-29.90	-30.27	-30.49	-30.53	-30.82
2	-30.27	-30.34	-30.31	-30.79	-31.00
3	-30.88	-30.74	-30.61	-30.05	-30.26
4	-31.07	-30.77	-30.71	-30.75	-30.04
Delta	1.16	0.50	0.40	0.74	0.96
Rank	1	4	5	3	2

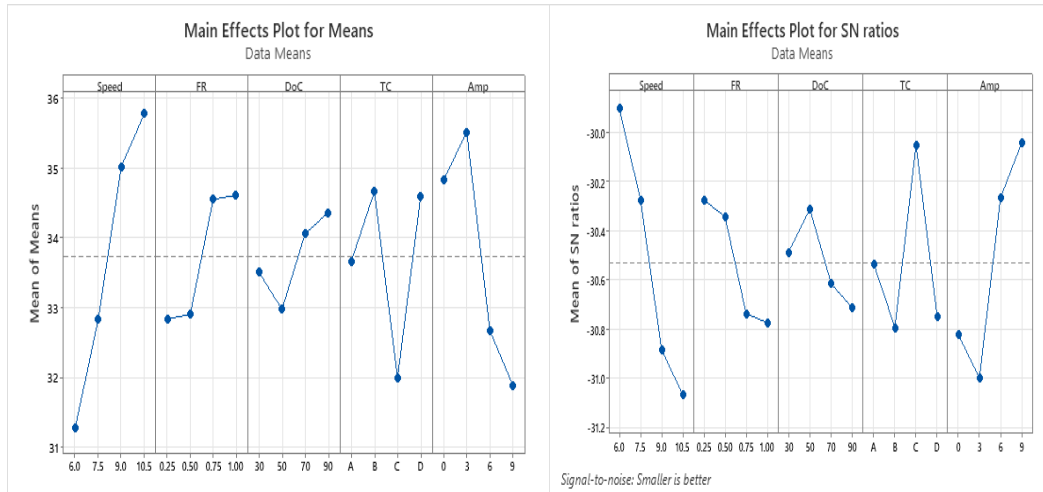


Figure 4.4: Main Effect Plots for Means and S/N Ratios of Tool Wear

The aforementioned statistical findings demonstrate that tool wear is impacted by each of the criteria that were chosen. While feed rate and depth of cut are minor considerations, cutting speed, amplitude, and type of coating have a considerable effect on tool wear. The results of tool wear analysis are summarized as:

- The most important factor that directly affects tool wear is cutting speed. The friction between the tool and the material of the workpiece causes the operating temperature to rise at greater speeds, which can lead to the thermal or diffusion wear of the tool. Also, chemical reactivity of tool material with workpiece material can increase at elevated temperature. This phenomenon can also accelerate the tool wear at high temperature.
- At higher amplitudes, the total dwell time and the average cutting forces are reduced. These phenomena affect tool wear positively, hence, reducing tool wear at higher amplitudes.
- TiAlN is aluminum-based tool coating, which has a low thermal stability as compared to TiSiN and nAlCo. Also, TiAlN is comparatively less stable to withstand the abrasive nature of harder materials like Inconel 718 for longer times. As a result, TiAlN coated tools are easy to wear.
- As the above analysis indicates, larger feed rates often result in higher cutting forces and increased temperatures, which hasten tool wear. As the depth of the cut grows, so does tool wear, as shown in Figure 4.2. This is also because of elevated temperatures at increased depths. A slight elevation in tool wear at lowest depth is due to the roughness of the laser slots surfaces.

4.4 Burr Formation

According to Mian et al. [101], the most important element influencing burr thickness is feed rate. Additionally, in micro-milling, the cutting edge's diameter is vital [102, 103], as increased cutting-edge's diameter increase cutting pressure, and wider burrs are formed [12, 104]. Burr formation occurs in both; down milling and up milling having different burr height and burr width [105]. Parts of

magnified images of slots from all experiments are collected in Figure 4.5 to show the burr formation.

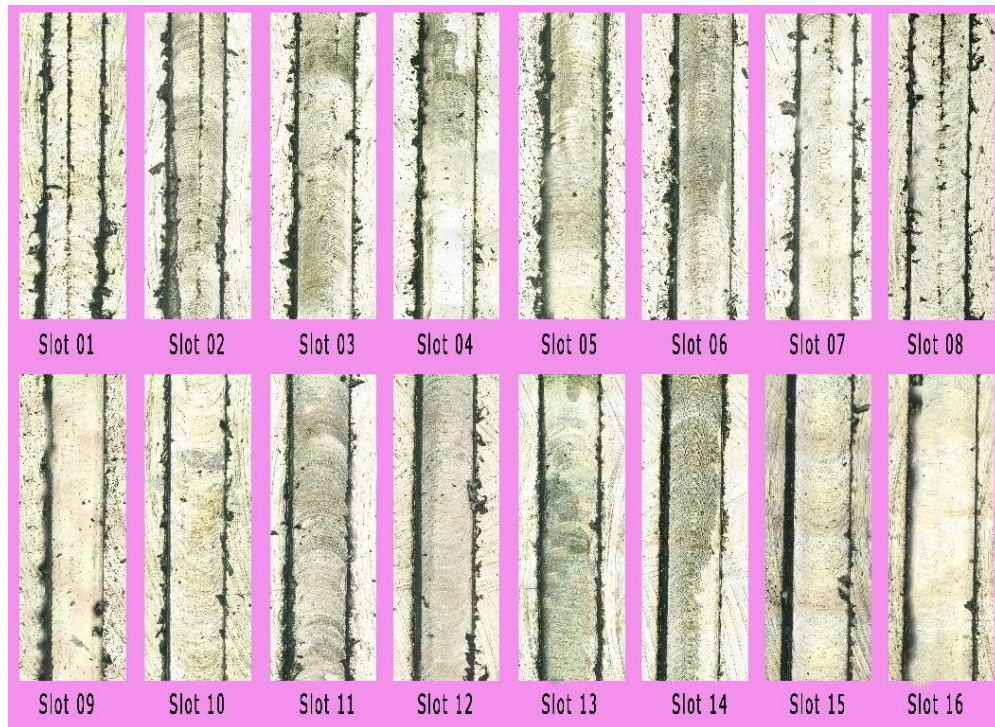


Figure 4.5: Burr Formation in All Experimental Runs

ANOVA was performed for all the four responses related to burr formation, including Burr Width in Down Milling (BWDM), Burr Height in Down Milling (BHDM), Burr Width in Up Milling (BWUM) and Burr Height in Up Milling (BHUM). Effect of the selected factors on all the four responses is depicted in Table 4.7- 4.10.

Table 4.7: Analysis of Variance for BWDM

Source	DF	Seq SS	Contribution	Adj SS	Adj MS	F-Value	P-Value
Regression	7	6176.5	82.39%	6176.5	882.4	5.35	0.015
Speed	1	3060.3	40.82%	3060.3	3060.3	18.54	0.003
FR	1	238.0	3.18%	238.0	238.0	1.44	0.264
DoC	1	2416.9	32.24%	2416.9	2416.9	14.64	0.005
Amp	1	156.8	2.09%	156.8	156.8	0.95	0.358
TC	3	304.5	4.06%	304.5	101.5	0.61	0.624
Error	8	1320.3	17.61%	1320.3	165.0		
Total	15	74968	100%				

Table 4.8: Analysis of Variance for BHDM

Source	DF	Seq SS	Contribution	Adj SS	Adj MS	F-Value	P-Value
Regression	7	5572.83	88.40%	5572.83	796.12	8.71	0.003
Speed	1	2806.48	44.52%	2806.48	2806.48	30.70	0.001
FR	1	2.38	0.04%	2.38	2.38	0.03	0.876
DoC	1	1414.83	22.44%	1414.83	1414.83	15.48	0.004
Amp	1	526.15	8.35%	526.15	526.15	5.76	0.043
TC	3	822.98	13.05%	822.98	274.33	3.00	0.095
Error	8	731.37	11.60%	731.37	91.42		
Total	15	6304.20	100%				

Table 4.9: Analysis of Variance for BWUM

Source	DF	Seq SS	Contribution	Adj SS	Adj MS	F-Value	P-Value
Regression	7	8242.8	82.63%	8242.8	1177.5	5.44	0.015
Speed	1	1941.6	19.468%	1941.6	1941.6	8.97	0.017
FR	1	2007.9	20.13%	2007.9	2007.9	9.27	0.016
DoC	1	3403.2	34.12%	3403.2	3403.2	15.71	0.004
Amp	1	415.4	4.16%	415.4	415.4	1.92	0.203
TC	3	474.6	4.76%	474.6	158.2	0.73	0.562
Error	8	1732.6	17.37%	1732.6	216.6		
Total	15	9975.4	100%				

Table 4.10: Analysis of Variance for BHUM

Source	DF	Seq SS	Contribution	Adj SS	Adj MS	F-Value	P-Value
Regression	7	7321.2	89.28%	7321.2	1045.88	9.52	0.002
Speed	1	1547.0	18.78%	1547.0	1547.0	14.08	0.006
FR	1	2440.6	29.76%	2440.6	2440.6	22.21	0.002
DoC	1	2508.5	30.59%	2508.5	2508.45	22.83	0.001
Amp	1	708.3	8.64%	708.3	708.32	6.45	0.035
TC	3	116.8	1.42%	116.8	38.92	0.35	0.788
Error	8	879.2	10.72%	879.2	109.90		
Total	15	8200.4	100%				

Each response was additionally analyzed for obtaining the response tables for means and S/N ratios individually. At last, all the burr formation responses were collectively analyzed for means and S/N ratios. Table 4.11 - 4.20 shows the individual and collective Main Effect Plots for all the responses.

Table 4.11: Response Table for Means of BWDM

Level	Speed	FR	DoC	TC	Amp
1	149.2	174.2	154.9	165.2	168.5
2	167.7	179.7	161.5	177.0	164.7
3	182.5	162.5	184.5	169.5	178.5
4	185.5	168.5	183.9	173.2	173.2
Delta	36.3	17.2	29.6	11.8	13.7
Rank	1	3	2	5	4

Table 4.112: Response Table for S/N Ratios of BWDM

Level	Speed	FR	DoC	TC	Amp
1	-43.43	-44.65	-43.75	-44.24	-44.41
2	-44.48	-45.02	-44.15	-44.88	-44.29
3	-45.20	-44.21	-45.29	-44.54	-44.97
4	-45.29	-44.52	-45.22	-44.75	-44.73
Delta	1.86	0.80	1.53	0.64	0.69
Rank	1	3	2	5	4

Table 4.13: Response Table for Means of BHDM

Level	Speed	FR	DoC	TC	Amp
1	146.2	168.8	155.5	179.8	176.4
2	173.0	171.0	166.7	171.6	175.5
3	172.3	169.4	174.0	160.7	161.7
4	185.9	168.2	181.2	165.3	163.9
Delta	39.7	2.8	25.6	19.1	14.7
Rank	1	5	2	3	4

Table 4.114: Response Table for S/N Ratios of BHDM

Level	Speed	FR	DoC	TC	Amp
1	-43.29	-44.50	-43.83	-45.04	-44.89
2	-44.69	-44.60	-44.41	-44.65	-44.84
3	-44.71	-44.47	-44.72	-44.07	-44.09
4	-45.37	-44.49	-45.10	-44.32	-44.23
Delta	2.08	0.13	1.28	0.97	0.80
Rank	1	5	2	3	4

Table 4.15: Response Table for Means of BWUM

Level	Speed	FR	DoC	TC	Amp
1	136.2	139.4	126.4	154.1	143.5
2	133.3	131.8	142.6	149.4	144.4
3	160.6	153.3	155.6	147.7	142.9
4	160.0	165.6	165.5	139.0	159.2
Delta	27.3	33.8	39.2	15.0	16.4
Rank	3	2	1	5	4

Table 4.116: Response Table for S/N Ratios of BWUM

Level	Speed	FR	DoC	TC	Amp
1	-42.52	-42.78	-41.74	-43.61	-43.04
2	-42.22	-42.06	-42.98	-43.39	-43.12
3	-44.10	-43.70	-43.82	-43.36	-42.75
4	-44.07	-44.36	-44.37	-42.54	-43.99
Delta	1.88	2.31	2.63	1.06	1.23
Rank	3	2	1	5	4

Table 4.17: Response Table for Means of BHUM

Level	Speed	FR	DoC	TC	Amp
1	62.69	57.14	52.23	73.83	81.29
2	59.25	59.05	69.21	73.94	70.52
3	76.68	82.49	76.11	68.04	72.08
4	86.20	86.15	87.27	69.01	60.93
Delta	26.95	29.01	35.03	5.91	20.36
Rank	3	2	1	5	4

Table 4.18: Response Table for S/N Ratios of BHUM

Level	Speed	FR	DoC	TC	Amp
1	-35.62	-34.37	-33.69	-36.98	-37.73
2	-34.06	-34.64	-35.81	-37.09	-36.78
3	-37.55	-38.17	-37.56	-35.97	-36.22
4	-38.62	-38.68	-38.81	-35.81	-35.12
Delta	4.56	4.31	5.12	1.28	2.61
Rank	2	3	1	5	4

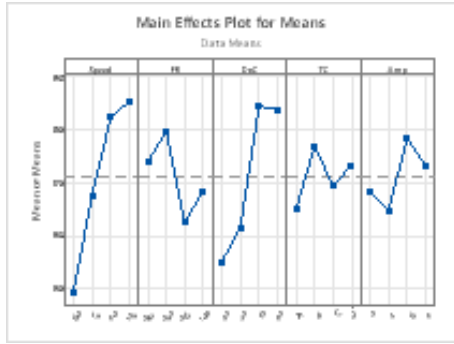
Table 4.119: Response Table for Collective Means of BWDM, BHDM, BWUM and BHUM

Level	Speed	FR	DoC	TC	Amp
1	123.6	134.9	122.3	143.2	142.4
2	133.3	135.4	135.0	143.0	138.8
3	148.0	141.9	147.5	136.5	138.8
4	154.4	147.1	154.5	136.6	139.3
Delta	30.8	12.2	32.2	6.8	3.6
Rank	2	3	1	4	5

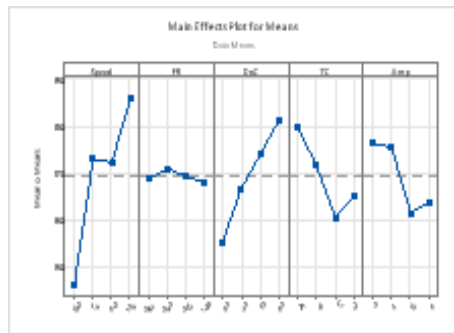
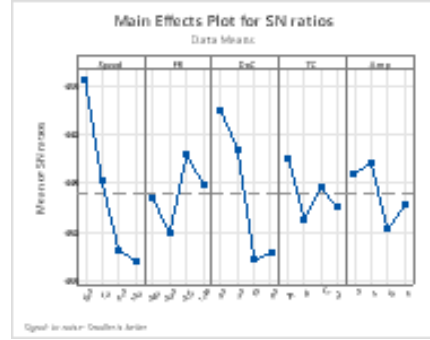
Table 4.20: Response Table for Collective S/N Ratios of BWDM, BHDM, BWUM and BHUM

Level	Speed	FR	DoC	TC	Amp
1	-42.19	-43.01	-42.26	-43.40	-43.29
2	-42.99	-43.07	-42.96	-43.40	-43.19
3	-43.75	-43.30	-43.71	-43.06	-43.19
4	-44.06	-43.60	-44.06	-43.13	-43.31
Delta	1.87	0.59	1.81	0.34	0.12
Rank	1	3	2	4	5

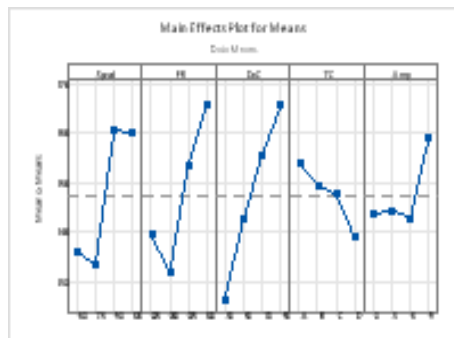
As minimizing the burr formation was one of the objectives of the study, therefore ‘smaller is the better’ criteria was used for calculating the S/N ratios of all the responses, related to burr formation. Information in the individual response tables is graphically represented in Figure 4.6, while that of collective response tables is shown in Figure 4.7.



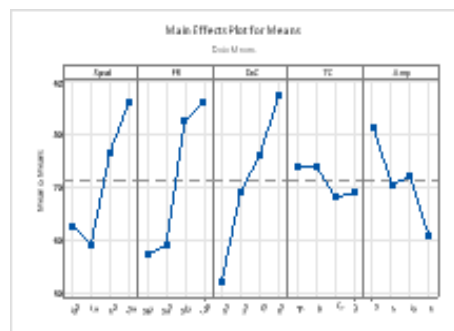
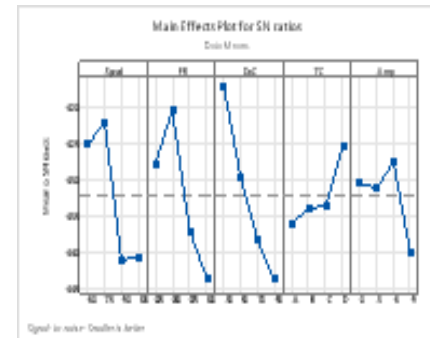
e.



f.



g.



h.

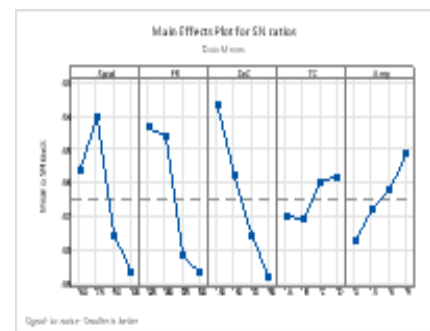


Figure 4.6: Main Effect Plots for Means (a, b, c and d) and Main Effect Plots for S/N Ratios (e, f, g and h) of BWDM, BHDM, BWUM and BHUM

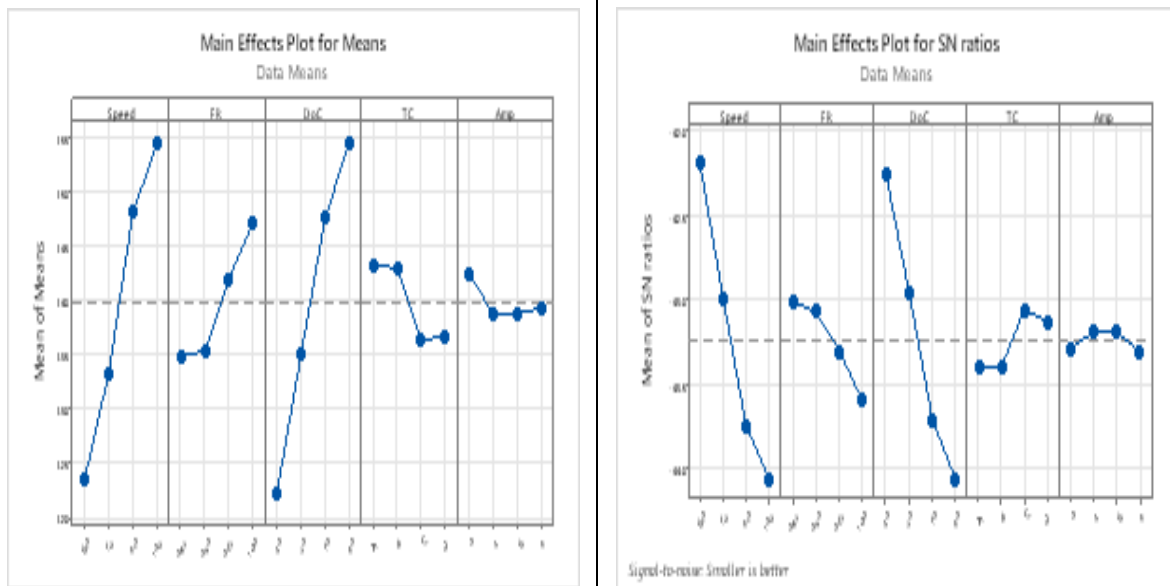


Figure 4.7: Collective Main Effect Plots of Means and S/N Ratios of BWDM, BHDM, BWUM and BHUM

It is evident from the above analysis that all the selected factors are contributing to impact the width and height of both types of burr formations. Cutting speed and depth of cut are major contributors, while the other three factors are slightly significant. The results of collective Main Effect Plots can be summarized as:

- Speed has a direct relation with the burr formation. Low burrs are formed at lower speed, but increases as the speed is increased [106, 107]. As the cutting speed increases, the cutting temperature rises accordingly due to frictional forces. The rise in temperature leads to bending of tool's cutting edge, which widens the burrs [103, 108].
- As the depth of cut increases, so do the burrs. A greater amount of material is removed per unit length of cut as the depth rises. The increased material removal can result in higher cutting forces acting on the workpiece, causing more plastic deformation and burr formation. Also, a larger cut generates more heat, which can contribute to enhance burr formation.
- By increasing the feed rate, burr formation is increased consequently. As the feed increases, the cutting tool engages more rapidly with the tool material. This can lead to higher cutting forces, causing plastic deformation in the workpiece material, which can lead to grow burrs.
- A slight difference in burr formation due to tool coating is because of coefficient of friction of the tool's coating. At higher frictional coefficient, material deformation increases which can upsurge the burr formation [12, 103, 108]. By raising the vibration's amplitude, chip size may be decreased in terms of amplitude. This may lead to a higher frequency of chip breakage and a smaller burr size. [109, 110].

4.5 Mono-Objective Optimization

Optimization of individual responses is carried out based on S/N ratios. In this study, we have same objective functions, i.e., to minimize SR, TW, BDM and BUM. Therefore, ‘smaller is the better’ criterion was applied for S/N ratios by using Equation (1). For all responses, average value of S/N ratios at each level were calculated. As the higher value of S/N ratio shows good response characteristics and vice versa, the best and worst responses of cutting parameters were found out, as shown in Table 4.21.

Table 4.21: Average S/N Ratios for SR, TW, BDM and BUM

Exp. #	Speed (m/min)	Feed ($\mu\text{m}/\text{tooth}$)	Depth of Cut (μm)	Tool Coating	Amplitude (μm)	SNR SR	SNR TW	SNR BDM	SNR BUM
1	6	0.25	30	Uncoated	0	23.742	-29.890	-43.485	-32.539
2	6	0.5	50	TiAlN	3	22.975	-30.219	-43.729	-34.081
3	6	0.75	70	TiSiN	6	24.883	-29.440	-42.579	-37.683
4	6	1	90	nACo	9	25.849	-30.054	-43.365	-38.195
5	7.5	0.25	50	TiSiN	9	26.936	-28.826	-43.848	-29.470
6	7.5	0.5	30	nACo	6	24.583	-29.991	-43.467	-28.563
7	7.5	0.75	90	Uncoated	3	24.013	-31.131	-46.081	-38.941
8	7.5	1	70	TiAlN	0	19.914	-31.150	-45.377	-39.267
9	9	0.25	70	nACo	3	30.173	-31.393	-45.030	-36.210
10	9	0.5	90	TiSiN	0	28.519	-30.685	-45.305	-38.841
11	9	0.75	30	TiAlN	9	24.731	-30.814	-43.823	-35.772
12	9	1	50	Uncoated	6	25.849	-30.641	-44.678	-39.382
13	10.5	0.25	90	TiAlN	6	26.936	-30.985	-45.655	-39.257
14	10.5	0.5	70	Uncoated	9	29.370	-30.473	-45.898	-37.060
15	10.5	0.75	50	nACo	0	24.293	-31.556	-45.403	-40.289
16	10.5	1	30	TiSiN	3	24.152	-31.246	-44.530	-37.876
Maximum SNR Value						30.173	-28.826	-42.579	-28.563
Minimum SNR Value						19.914	-31.556	-46.081	-40.289

From the above table, it can be concluded that:

- Experiment 09 results in best surface quality (Speed = 9, Feed = 0.25, DoC = 70 and Amp. = 3 with nACo coated tool) and Experiment 8 results in worst surface quality (Speed = 7.5, Feed = 1, DoC = 70 and Amp. = 0 with TiAlN coated tool).

- Experiment 05 results in minimizing tool wear (Speed = 7.5, Feed = 0.25, DoC = 50 and Amp. = 9 with TiSiN coated tool) and Experiment 15 results in maximizing it (Speed = 10.5, Feed = 0.75, DoC = 50 and Amp. = 0 with nACo coated tool).
- Experiment 03 results in minimization of burr formation in down milling (Speed = 6, Feed = 0.75, DoC = 70 and Amp. = 6 with TiSiN coated tool) and Experiment 07 results in its maximization (Speed = 7.5, Feed = 0.75, DoC = 90 and Amp. = 3 with Uncoated tool).
- Experiment 06 results in minimization of burr formation in up milling (Speed = 7.5, Feed = 0.5, DoC = 30 and Amp. = 6 with nACo coated tool) and Experiment 15 results in its maximization (Speed = 10.5, Feed = 0.75, DoC = 50 and Amp. = 0 with nACo coated tool).

CHAPTER 5: MULTI OBJECTIVE OPTIMIZATION

5.1 Multi Response Optimization

In Chapter 4, mono-objective optimization was carried out for all the responses individually, including surface roughness, tool wear, burr formation in down milling and burr formation in up milling, on the basis of average S/N ratios. All the results of single response optimization are summarized in Figure 5.1.

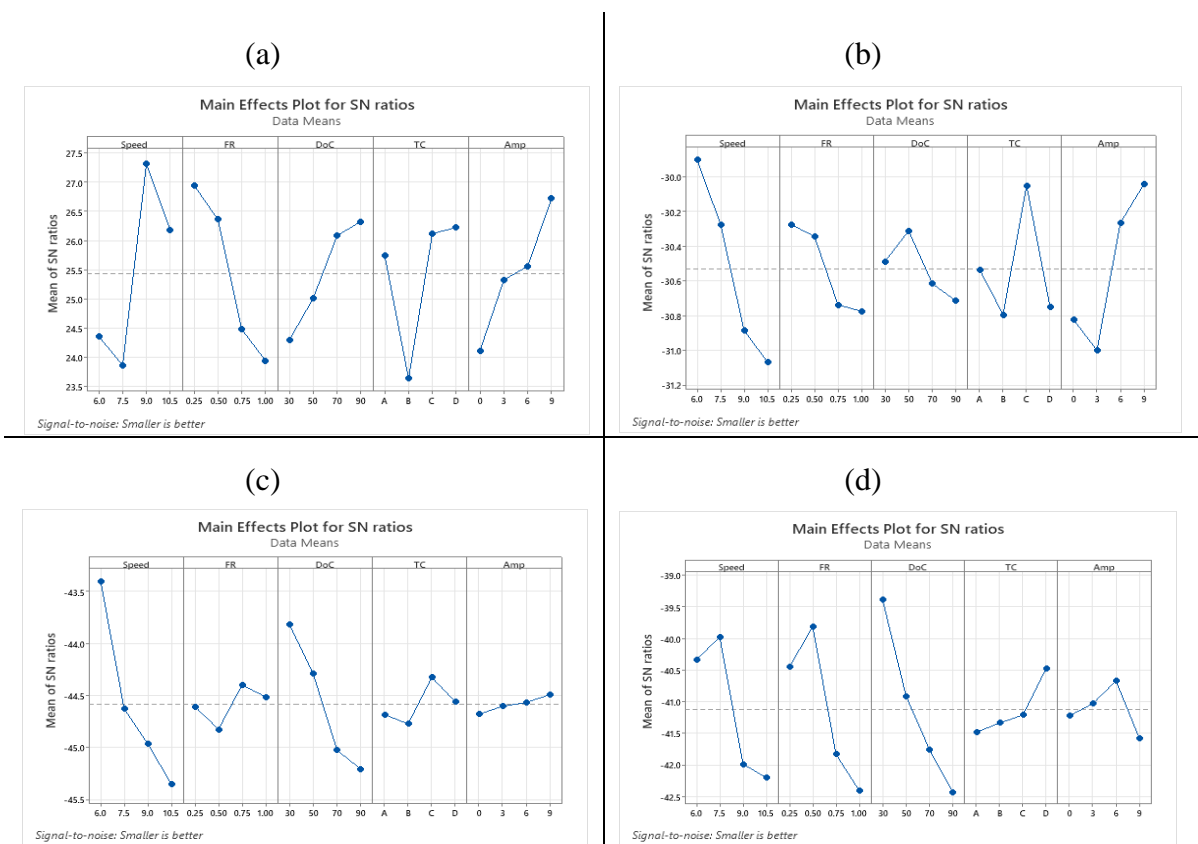


Figure 5.1: Main Effect Plots for S/N Ratios of (a) SR, (2) TW, (3) BDM and (4) BUM

It is visible from the above figure that there is a huge inconsistency among the optimized values of responses, therefore, predicting the collective effect of all responses is improbable. In such cases, it is required to optimize the responses simultaneously by using Multi Objective Optimization (MOO) techniques [19, 111, 112]. This study has employed one of such techniques, namely, Grey Relational Analysis (GRA) [113, 114] coupled with Principal Component Analysis (PCA) [115, 116].

5.2 GRA-PCA

GRA is based on assigning equal weights to all response variables, which can negatively affect the process of decision making. To avoid this uncertainty, PCA was employed for assigning relative weights to each response variable [117]. GRA starts with Grey relational generation [118] involving the linear normalization of reference sequence (experimental data) in comparable sequence (range of 0 to 1). As the aim of this study was to minimize all the response variables, Equation (2) was used for data normalization.

$$y_j^*(q) = \frac{\max y_j(q) - y_j(q)}{\max y_j(q) - \min y_j(q)} \quad (2)$$

Where $y_j^*(q)$ = Grey relational value, $y_j(q)$ = corresponding average S/N ratio value, and $\max y_j(q)$ and $\min y_j(q)$ are the largest and smallest $y_j(q)$ values for the q^{th} observation, where q is the number of outputs. Of all the normalized values, best result will be equal to 1, therefore; a higher normalized value is expected for each better response. Following normalization of data, deviation sequence values were calculated by using Equation (3). All the normalized and deviation sequence values are shown in Table 5.1.

$$\Delta_{0i}(q) = |y_{0i}^*(q) - y(q)| \quad (3)$$

Where $y_{0i}^*(q)$ is the maximum of normalized values and $y(q)$ is the corresponding normalized value.

The next step was to find Grey Relational Constant (GRC) using Equation (4).

$$\xi(y_j^*(q), y_{0i}^*(q)) = \frac{\Delta_{\min}(q) + \zeta \Delta_{\max}(q)}{\Delta_{0j}(q) + \zeta \Delta_{\max}(q)} \quad (4)$$

Where ζ is the identification or distinguishing coefficient whose value is taken between 0 and 1, generally (and in this study) set at 0.5 [119]. For better final results, PCA was performed using Minitab-21 to assign weights to quality characteristics. Table 02 depicts PC values for all response variables.

Table 5.1: Data Grey Relational Generation and Deviation Sequence

Normalized Values					Deviation Sequence			
Exp.#	SR	TW	BDM	BUM	SR	TW	BDM	BUM
1	0.627	0.390	0.000	0.358	0.373	0.610	1.000	0.642
2	0.702	0.510	0.212	0.435	0.298	0.490	0.788	0.565
3	0.516	0.225	0.159	0.769	0.484	0.775	0.841	0.231
4	0.421	0.450	0.298	0.966	0.579	0.550	0.702	0.034
5	0.316	0.000	0.349	0.532	0.684	1.000	0.651	0.468
6	0.545	0.427	0.365	0.000	0.455	0.573	0.635	1.000
7	0.600	0.844	0.704	0.901	0.400	0.156	0.296	0.099
8	1.000	0.851	0.733	0.893	0.000	0.149	0.267	0.107
9	0.000	0.940	0.775	0.753	1.000	0.060	0.225	0.247
10	0.161	0.681	0.848	0.889	0.839	0.319	0.152	0.111
11	0.530	0.728	0.379	0.811	0.470	0.272	0.621	0.189
12	0.421	0.665	0.552	1.000	0.579	0.335	0.448	0.000
13	0.316	0.791	1.000	0.949	0.684	0.209	0.000	0.051
14	0.078	0.603	0.961	0.911	0.922	0.397	0.039	0.089
15	0.573	1.000	0.631	0.884	0.427	0.000	0.369	0.116
16	0.587	0.886	0.429	0.828	0.413	0.114	0.571	0.172

Table 5.2: Eigenvector Representing Weights for All Response Variables

Variable	PC1	PC2	PC3	PC4	(PC1) ²
SR	-0.093	-0.729	0.222	-0.641	0.008649
TW	0.502	-0.589	-0.457	0.438	0.252004
BDM	0.626	0.349	-0.344	-0.607	0.391876
BHM	0.59	0.016	0.789	0.17	0.3481
SUM	1.625				1.000629

As PC1 is the primary principal component showing the maximum variance in the data, its values were used for further processing. The sum of PC1 values, as Table 5.2 shows, is not equal to one. The squares of those values were taken whose sum was almost equalling 1, as shown in the above table. SR, TW, BDM and BHM were assigned the weights of 0.008649, 0.252004, 0.391876 and 0.3481 respectively.

After PCA, Weighted Grey Relational Grades (W-GRG) were calculated by using Equation (5) [120]. The weighted mean of the individual GRCs for each experiment is used to compute the correlation strength between the experimental runs, which is determined using GRG. The higher the W-GRG value, better will be the multi responses and vice versa. Ranking was done on the basis of this criteria; experiment with the highest W-GRG was allotted number 1, second highest with number 2, and so on [121]. All the GRC, W-GRG and Ranking data is depicted in Table 5.3 and following results were observed in this analysis:

- Experiment 13 has the highest value of GRG = 0.889. It means that; at Speed = 10.5, Feed = 0.25, DoC = 90 and Amplitude = 6 with TiAlN coated tool, the overall result will be the best.
- Experiment 01 has the lowest value of GRG = 0.401. It means that; at Speed = 6, Feed = 0.25, DoC = 30 and Amplitude = 0 with uncoated tool, the overall result will be the worst.

$$\gamma_j(y_0^*, y_j^*) = \frac{1}{n} \sum_{q=1}^n w_q \xi(y_j^*(q), y_0^*(q)) \quad (5)$$

Where n is the number of response variables, $\sum_{q=1}^n w_q = 1$, and w_q is weight of q^{th} response.

The W-GRG values were further analyzed for multi optimization purpose, by using Taguchi Design of Experiments. The optimal combination of factors was predicted by Table 5.4, showing response table for means on ‘Larger is Better’ criterion. Table 5.4 shows that The best outcomes are achieved when the machining parameters—such as feed, speed, and depth of cut—are at level 4, and amplitude is kept at level 3 with TiAlN coated tool.

Table 5.3: GRC and W-GRG Values for All Response Variables

Exp. #	GRC Values				W-GRG	Ranks
	SR	TW	BDM	BUM		
1	0.573	0.450	0.333	0.438	0.401	16
2	0.626	0.505	0.388	0.470	0.448	13
3	0.508	0.392	0.373	0.684	0.487	12
4	0.464	0.476	0.416	0.937	0.613	10
5	0.422	0.333	0.434	0.517	0.438	14
6	0.523	0.466	0.440	0.333	0.411	15
7	0.556	0.762	0.628	0.835	0.734	6
8	1.000	0.771	0.651	0.824	0.745	4
9	0.333	0.893	0.690	0.669	0.731	7
10	0.373	0.610	0.767	0.818	0.742	5
11	0.516	0.648	0.446	0.726	0.595	11
12	0.464	0.598	0.527	1.000	0.710	8
13	0.422	0.705	1.000	0.907	0.889	1
14	0.352	0.557	0.928	0.849	0.803	2
15	0.539	1.000	0.575	0.812	0.765	3
16	0.548	0.815	0.467	0.744	0.652	9

Table 5.4: Response Table for Means of W-GRG

Level	Speed	FR	DoC	TC	Amp
1	0.4876	0.6148	0.5149	0.6619	0.6635
2	0.5818	0.6010	0.5902	0.6694	0.6414
3	0.6947	0.6454	0.6916	0.5800	0.7441
4	0.7771	0.6800	0.7445	0.6299	0.5921
Delta	0.2896	0.0790	0.2296	0.0894	0.1520
Rank	1	5	2	4	3

5.3 Response Surface Methodology (RSM) and Regression Modelling (RM)

RSM performs statistical analysis to optimize and model complex processes involving multiple variables [122-124]. The technique was employed in this study for optimization and

Regression Modelling of W-GRG values. RM is another statistical technique which examines the relationship between dependent and independent variables [125, 126].

Firstly, ANOVA was conducted for the W-GRG values to find significantly contributing factors, and the results are compiled in Table 5.5. Further, a second-order RSM model was used to create a multi- objective W-GRG function that closely matches the experimentally produced W-GRG. Machining parameters, including speed, feed, depth of cut and amplitude, were continuous factors while tool coating was a non-continuous categorical factor in the current study. Tool Coating (TC) was contained of four different degrees, namely uncoated, TiAlN, TiSiN, nACo. A separate function, shown in Equation (6), (7), (8), and (9), for each TC degree was developed. Those equations were developed using response surface regression model with R-Square of 99.10% and R-Square Adjusted of 98.06%.

Table 5.5: Analysis of Variance for W-GRG

Source	DF	Seq SS	Contribution	Adj SS	Adj MS	F-Value	P-Value
Model	8	0.357128	99.10%	0.357128	0.044641	95.82	0.000
Linear	7	0.354779	98.44%	0.354779	0.050683	108.79	0.000
Speed	1	0.192670	43.46%	0.192670	0.192670	413.55	0.000
FR	1	0.011500	3.19%	0.011500	0.011500	24.68	0.002
DoC	1	0.124909	34.66%	0.124909	0.124909	268.11	0.000
Amp	1	0.005869	9.63%	0.005869	0.005869	12.60	0.001
TC	3	0.019830	7.50%	0.019830	0.006610	14.19	0.002
Square	1	0.002348	0.65%	0.002348	0.002348	5.04	0.060
FR*FR	1	0.002348	0.65%	0.002348	0.002348	5.04	0.060
Error	7	0.003261	0.90%	0.003261	0.000466		
Total	15	0.360389	100.00%				

Equations 6-9 predicted, by using response regression model, that the best performing non- continuous categorical factor would be TiAlN for the optimized solution. The generated model can only be used to laser-based ultrasonic aided micro milling of Inconel-718 with both

coated and uncoated tools under certain conditions: ($6 \text{ m/min} \leq \text{speed} \leq 10.5 \text{ m/min}$), ($0.25 \mu\text{m/tooth} \leq \text{feed} \leq \mu\text{m/tooth}$), ($30 \mu\text{m} \leq \text{DoC} \leq 90 \mu\text{m}$), ($0 \mu\text{m} \leq \text{amplitude} \leq 9 \mu\text{m}$).

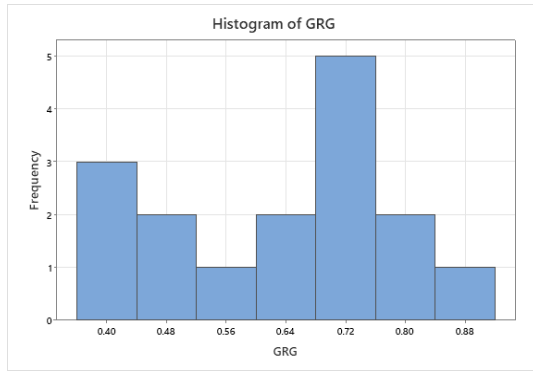
Table 5.6: Regression Equations for W-GRG (speed, FR, DoC, and Amp) with Different TCs

TC	Corresponding Regression Equation
nACo	$\begin{aligned} \text{W-GRG} = & -0.1207 + 0.06543 \text{ Speed} - 0.146 \text{ FR} + 0.003951 \text{ DoC} \\ & - 0.00571 \text{ Amp} \\ & + 0.1938 \text{ FR*FR} \end{aligned} \quad (6)$
TiAlN	$\begin{aligned} \text{W-GRG} = & -0.0812 + 0.06543 \text{ Speed} - 0.146 \text{ FR} + 0.003951 \text{ DoC} \\ & - 0.00571 \text{ Amp} \\ & + 0.1938 \text{ FR*FR} \end{aligned} \quad (7)$
TiSiN	$\begin{aligned} \text{W-GRG} = & -0.1706 + 0.06543 \text{ Speed} - 0.146 \text{ FR} + 0.003951 \text{ DoC} \\ & - 0.00571 \text{ Amp} \\ & + 0.1938 \text{ FR*FR} \end{aligned} \quad (8)$
Uncoated	$\begin{aligned} \text{W-GRG} = & -0.0887 + 0.06543 \text{ Speed} - 0.146 \text{ FR} + 0.003951 \text{ DoC} \\ & - 0.00571 \text{ Amp} \\ & + 0.1938 \text{ FR*FR} \end{aligned} \quad (9)$

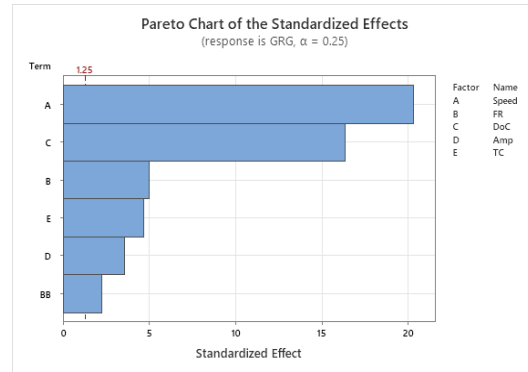
Using Response Surface Regression, histogram (Figure 5.2a) and normal probability plot (Figure 5.2b) were generated to show the normal distribution and scatter of the W-GRG data. Pareto Chart (Figure 5.2c) was created to show the effects of all factors, while Versus Order (Figure 5.2d) showed that there is no correlation existing among the factors. All the plots are combinedly presented in Figure 5.2.

5.4 Regression Model Optimization

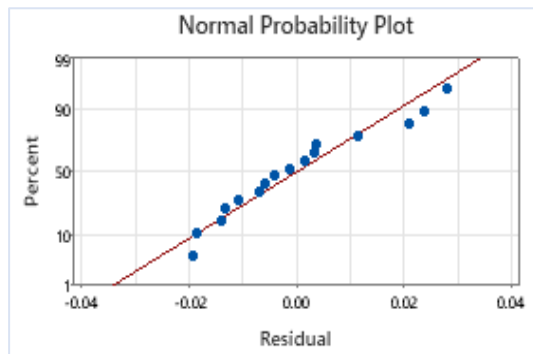
In order to get the best output results, the optimal set of machining settings was determined using the Response Surface Optimization statistical approach. [127]. With a 95% confidence level, the response surface optimizer projected the optimal parameter combination for maximized W-GRG, which would yield the lowest value of burr formation, tool wear, and surface roughness. [128]. The finally optimized results are depicted in Table 5.7, while Figure 5.3 graphically represents the multiple response predictions.



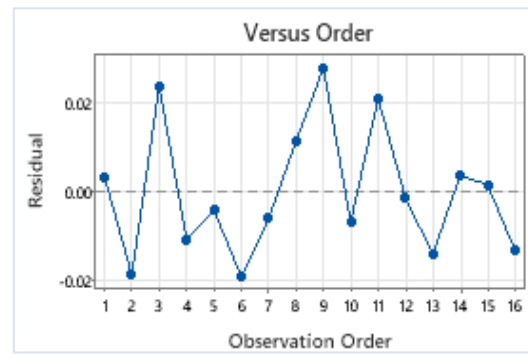
(a)



(b)



(c)



(d)

Figure 5.2: Response Surface Regression of W-GRG (a) Histogram; (b) Pareto Chart; (c) Normal Probability Plot for Residual; (d) Observation Order of Residual

Table 5.7: Multiple Response Prediction Along with Their Parameters

Parameters					
Response	Goal	Lower Value	Target	Weight	Importance
W-GRG	Maximum	0.401	0.889	1	1

Multiple Response Prediction

Variable	Speed	FR	DoC	TC	Amp.
Setting	7.18182	0.25	57.2727	TiA1N	9



Figure 5.3: Graph of Multiple Response Prediction

5.5 Result Validation

Parameters' values from multiple response prediction were used to carry out a validation experiment. The Response variables from that experiment were compared with the best results of initial trials' run (Experiment 13). Figure 5.4 shows workpiece after validation experiment, and Table 5.8 provides a comparison between the results of Experiment 13 and Final Validation Experiment.

Table 5.8: Comparison of Best Run and RSM Optimized Run

Exp. Name	Laser Cut	Speed	Feed	DoC	TC	Amp.	SR	TW	BDM	BUM
	(μm)	(m/min)	($\mu\text{m}/\text{tooth}$)	(μm)		(μm)	(μm)	(μm)	(μm)	(μm)
Best Run	20	10.5	0.25	90	TiAlN	6	0.045	35.42	191.754	91.802
RSM Optimized Run	20	7.182	0.25	57.273	TiAlN	9	0.041	28.397	151.177	109.431

It is evident from the above table, that the results have been improved significantly in RSM- optimized run, as compared to Experiment 13. The results show that surface quality has been improved by 19.83%, tool performance by 8.89%, BDM has been reduced by 21.16%, while BUM has been increased by 19.20%.

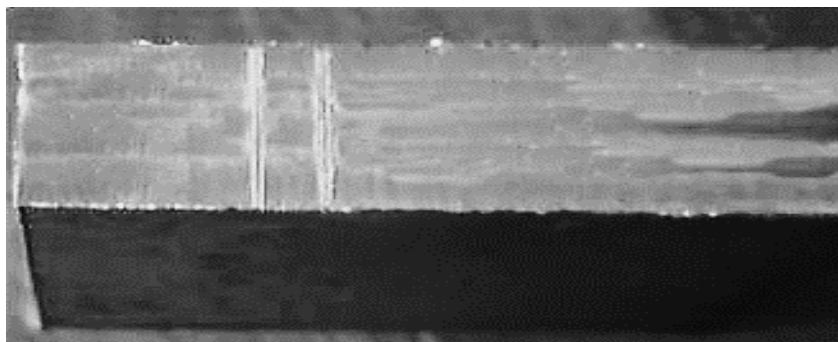


Figure 5.4: Workpiece After RSM-Optimized Run

CHAPTER 6: CONCLUSION AND FUTURE RECOMMENDATIONS

6.1 Conclusions

In this work, Inconel 718 was micro milled using a variety of machining parameters (speed, feed, depth of cut, amplitude of tool vibration, and tool coating), utilizing both conventional micro milling and ultrasonic-assisted low-speed micro milling that was based on laser pre-slotting. We looked at how those machining parameters affected surface roughness, burr formation, and tool wear. The following summarizes the primary conclusions:

- All the response variables including surface roughness, tool wear, and particularly burr formation can all be significantly improved with LLUMM, however, the probability of improving surface quality for lower depth of cut is very low.
- Better results can be obtained through LLUMM by applying lower feed, higher speed and larger amplitude of tool vibration.
- TiAlN is the best tool coating in LLUMM to machine Inconel-718, while the overall effect of tool coating on output responses is 7.50%.
- Cutting speed and depth of cut are the dominant factors in LLUMM, having 43.46% and 34.66% respective effectiveness on the output variables, followed by amplitude of tool vibration with 9.63% effect.
- Output responses in LLUMM are not much affected by feed rate, as it has the least impact of only 3.19%
- Instead of compromising the overall product quality through unnecessary processes of deburring, LLUMM negates such operations and produces better results for surface roughness, tool wear, and burr development.
- This work backs the low-speed machining of Inconel-718 and other challenging-to-machine materials using sophisticated machining methods like LLUMM.
- This research also demonstrates the viability of laser-assist in micro machining; not only for 10 pre-heating, but for cutting too.

6.2 Future Recommendations

- This study can help to study LLUMM for lower depth of cuts by considering laser-slotting as a variable factor.
- This work can be used for explaining the machining forces in LLUMM
- The RSM-optimized machining parameters, obtained from this work, can be tested for other super alloys.
- This research can help to optimize other machining parameters like material removal rate, cutting forces, cutting energy, and tool diameter etc. for Inconel-718 and other super alloys.
- Machining timing for super alloys, especially Nickle alloys like Inconel-718, can also be investigated with the help of this study.

References

- [1] F. Schneider, J. Das, B. Kirsch, B. Linke, and J. C. Aurich, "Sustainability in ultra precision and micro machining: A review," *International Journal of Precision Engineering and Manufacturing-Green Technology*, vol. 6, pp. 601-610, 2019.
- [2] M. Hasan, J. Zhao, and Z. Jiang, "Micromanufacturing of composite materials: a review," *International Journal of Extreme Manufacturing*, vol. 1, no. 1, p. 012004, 2019.
- [3] S. Ruggeri, G. Fontana, and I. Fassi, "Micro-assembly," *Micro-Manufacturing Technologies and Their Applications: A Theoretical and Practical Guide*, pp. 223-259, 2017.
- [4] H. Fallahi, J. Zhang, H.-P. Phan, and N.-T. Nguyen, "Flexible microfluidics: Fundamentals, recent developments, and applications," *Micromachines*, vol. 10, no. 12, p. 830, 2019.
- [5] D. Petit, C. Faulkner, S. Johnstone, D. Wood, and R. Cowburn, "Nanometer scale patterning using focused ion beam milling," *Review of scientific instruments*, vol. 76, no. 2, 2005.
- [6] D. J. Guckenberger, T. E. De Groot, A. M. Wan, D. J. Beebe, and E. W. Young, "Micromilling: a method for ultra-rapid prototyping of plastic microfluidic devices," *Lab on a Chip*, vol. 15, no. 11, pp. 2364-2378, 2015.
- [7] H. Jansen and H. Gardeniers, "Meint de Boer, Miko Elwenspoek, and Jan Fluitman. A survey on the reactive ion etching of silicon in microtechnology," *Journal of micromechanics and microengineering*, vol. 6, no. 1, p. 14, 1996.
- [8] I. Utke, P. Hoffmann, and J. Melngailis, "Gas-assisted focused electron beam and ion beam processing and fabrication," *Journal of Vacuum Science & Technology B: Microelectronics and Nanometer Structures Processing, Measurement, and Phenomena*, vol. 26, no. 4, pp. 1197-1276, 2008.
- [9] F. Karouta, "A practical approach to reactive ion etching," *Journal of Physics D: Applied Physics*, vol. 47, no. 23, p. 233501, 2014.
- [10] A. A. Tseng, "Recent developments in micromilling using focused ion beam technology," *Journal of micromechanics and microengineering*, vol. 14, no. 4, p. R15, 2004.
- [11] G. Peake *et al.*, "A micromachined, shadow-mask technology for the OMVPE fabrication of integrated optical structures," *Journal of Electronic Materials*, vol. 29, pp. 86-90, 2000.
- [12] L.-h. Xu, H.-b. Na, and G.-c. Han, "Machinability improvement with ultrasonic vibration-assisted micro-milling," *Advances in Mechanical Engineering*, vol. 10, no. 12, p. 1687814018812531, 2018.
- [13] W. Betteridge and S. Shaw, "Development of superalloys," *Materials science and technology*, vol. 3, no. 9, pp. 682-694, 1987.
- [14] P. Caron and T. Khan, "Evolution of Ni-based superalloys for single crystal gas turbine blade applications," *Aerospace Science and Technology*, vol. 3, no. 8, pp. 513-523, 1999.

- [15] J. C. Williams and E. A. Starke Jr, "Progress in structural materials for aerospace systems," *Acta materialia*, vol. 51, no. 19, pp. 5775-5799, 2003.
- [16] W. Xia, X. Zhao, L. Yue, and Z. Zhang, "Microstructural evolution and creep mechanisms in Ni-based single crystal superalloys: A review," *Journal of Alloys and Compounds*, vol. 819, p. 152954, 2020.
- [17] J. Tlustý, "Dynamics of high-speed milling," 1986.
- [18] F. Alexandre, "Probabilistic and microstructural aspects of fatigue cracks initiation in Inconel 718," Ecole Nationale Supérieure des Mines, 2004.
- [19] W. Frifita, S. B. Salem, A. Haddad, and M. A. Yallese, "Optimization of machining parameters in turning of Inconel 718 Nickel-base super alloy," *Mechanics & Industry*, vol. 21, no. 2, p. 203, 2020.
- [20] M. A. Yallese, L. Boulanouar, and K. Chaoui, "Usinage de l'acier 100Cr6 trempé par un outil en nitrure de bore cubique," *Mécanique & Industries*, vol. 5, no. 4, pp. 355-368, 2004.
- [21] Z. Hessainia, A. Belbah, M. A. Yallese, T. Mabrouki, and J.-F. Rigal, "On the prediction of surface roughness in the hard turning based on cutting parameters and tool vibrations," *Measurement*, vol. 46, no. 5, pp. 1671-1681, 2013.
- [22] M. W. Azizi, S. Belhadi, M. A. Yallese, T. Mabrouki, and J.-F. Rigal, "Surface roughness and cutting forces modeling for optimization of machining condition in finish hard turning of AISI 52100 steel," *Journal of mechanical science and technology*, vol. 26, pp. 4105-4114, 2012.
- [23] W. Chen, X. Teng, L. Zheng, W. Xie, and D. Huo, "Burr reduction mechanism in vibration-assisted micro milling," *Manufacturing letters*, vol. 16, pp. 6-9, 2018.
- [24] B. M. Abdo, S. H. Mian, A. El-Tamimi, H. Alkhalefah, and K. Moiduddin, "Micromachining of biolox forte ceramic utilizing combined laser/ultrasonic processes," *Materials*, vol. 13, no. 16, p. 3505, 2020.
- [25] M. Hafiz *et al.*, "Machinability ultrasonic assisted milling of Inconel 718 by using Taguchi method," *ARPJ. Eng. Appl. Sci*, vol. 13, 2006.
- [26] C. Nath and M. Rahman, "Effect of machining parameters in ultrasonic vibration cutting," *International Journal of Machine Tools and Manufacture*, vol. 48, no. 9, pp. 965-974, 2008.
- [27] V. Jain, A. K. Sharma, and P. Kumar, "Recent developments and research issues in microultrasonic machining," *International Scholarly Research Notices*, vol. 2011, 2011.
- [28] Y. Su and L. Li, "Surface integrity of ultrasonic-assisted dry milling of SLM Ti6Al4V using polycrystalline diamond tool," *The International Journal of Advanced Manufacturing Technology*, pp. 1-10, 2022.
- [29] S. Zhang, S. To, S. Wang, and Z. Zhu, "A review of surface roughness generation in ultra-precision machining," *International Journal of Machine Tools and Manufacture*, vol. 91, pp. 76-95, 2015.
- [30] H. Wang, L. Li, S. Zhu, Y. Xu, and N. Ren, "Effect of water-based ultrasonic vibration on the quality of laser trepanned microholes in nickel super-alloy workpieces," *Journal of Materials Processing Technology*, vol. 272, pp. 170-183, 2019.

- [31] X.-X. Zhu, W.-H. Wang, R.-S. Jiang, Z.-F. Zhang, B. Huang, and X.-W. Ma, "Research on ultrasonic-assisted drilling in micro-hole machining of the DD6 superalloy," *Advances in Manufacturing*, vol. 8, pp. 405-417, 2020.
- [32] Y. Wu, Q. Wang, S. Li, and D. Lu, "Ultrasonic Assisted Machining of Nickel-Based Superalloy Inconel 718," in *Superalloys for Industry Applications*: IntechOpen, 2018.
- [33] E. Kaya and B. Akyüz, "Effects of cutting parameters on machinability characteristics of Ni-based superalloys: a review," *Open Engineering*, vol. 7, no. 1, pp. 330-342, 2017.
- [34] M. Sarıkaya, V. Yılmaz, and A. Güllü, "Analysis of cutting parameters and cooling/lubrication methods for sustainable machining in turning of Haynes 25 superalloy," *Journal of Cleaner Production*, vol. 133, pp. 172-181, 2016.
- [35] S. Darwish, "The impact of the tool material and the cutting parameters on surface roughness of supermet 718 nickel superalloy," *Journal of Materials Processing Technology*, vol. 97, no. 1-3, pp. 10-18, 2000.
- [36] D. Tali, "Machinability of Rene 41 Superalloy on Different Turning Parameters," ed: Eskisehir Osmangazi University Eskisehir, Turkey, 2016.
- [37] M. Sarıkaya and A. Güllü, "Taguchi design and response surface methodology based analysis of machining parameters in CNC turning under MQL," *Journal of Cleaner Production*, vol. 65, pp. 604-616, 2014.
- [38] D. D'addona, S. J. Raykar, and M. Narke, "High speed machining of Inconel 718: tool wear and surface roughness analysis," *Procedia CIRP*, vol. 62, pp. 269-274, 2017.
- [39] D. Dudzinski, A. Devillez, A. Moufki, D. Larrouquere, V. Zerrouki, and J. Vigneau, "A review of developments towards dry and high speed machining of Inconel 718 alloy," *International journal of machine tools and manufacture*, vol. 44, no. 4, pp. 439-456, 2004.
- [40] W. Grzesik, P. Niesłony, W. Habrat, J. Sieniawski, and P. Laskowski, "Investigation of tool wear in the turning of Inconel 718 superalloy in terms of process performance and productivity enhancement," *Tribology International*, vol. 118, pp. 337-346, 2018.
- [41] W. Akhtar, J. Sun, P. Sun, W. Chen, and Z. Saleem, "Tool wear mechanisms in the machining of Nickel based super-alloys: A review," *Frontiers of Mechanical Engineering*, vol. 9, pp. 106-119, 2014.
- [42] D. Teixidor, F. Orozco, T. Thepsonthi, J. Ciurana, C. A. Rodríguez, and T. Özel, "Effect of process parameters in nanosecond pulsed laser micromachining of PMMA-based microchannels at near-infrared and ultraviolet wavelengths," *The International Journal of Advanced Manufacturing Technology*, vol. 67, pp. 1651-1664, 2013.
- [43] S. Prakash and S. Kumar, "Experimental investigations and analytical modeling of multi-pass CO₂ laser processing on PMMA," *Precision Engineering*, vol. 49, pp. 220-234, 2017.
- [44] R. McCann, K. Bagga, R. Groarke, A. Stalcup, M. Vázquez, and D. Brabazon, "Microchannel fabrication on cyclic olefin polymer substrates via 1064 nm Nd: YAG laser ablation," *Applied Surface Science*, vol. 387, pp. 603-608, 2016.
- [45] S. Prakash and S. Kumar, "Fabrication of microchannels on transparent PMMA using CO₂ Laser (10.6 μm) for microfluidic applications: An experimental investigation," *International Journal of Precision Engineering and Manufacturing*, vol. 16, pp. 361-366, 2015.

- [46] D. Nieto, T. Delgado, and M. T. Flores-Arias, "Fabrication of microchannels on soda-lime glass substrates with a Nd: YVO₄ laser," *Optics and Lasers in Engineering*, vol. 63, pp. 11-18, 2014.
- [47] E. Bulushev, V. Bessmeltsev, A. Dostovalov, N. Goloshevsky, and A. Wolf, "High-speed and crack-free direct-writing of microchannels on glass by an IR femtosecond laser," *Optics and Lasers in Engineering*, vol. 79, pp. 39-47, 2016.
- [48] T.-L. Chang, Z.-C. Chen, Y.-W. Lee, Y.-H. Li, and C.-P. Wang, "Ultrafast laser ablation of soda-lime glass for fabricating microfluidic pillar array channels," *Microelectronic Engineering*, vol. 158, pp. 95-101, 2016.
- [49] V. Tangwarodomnukun and T. Wuttisarn, "Evolution of milled cavity in the multiple laser scans of titanium alloy under a flowing water layer," *The International Journal of Advanced Manufacturing Technology*, vol. 92, pp. 293-302, 2017.
- [50] S. Darwish, N. Ahmed, A. M. Alahmari, and N. A. Mufti, "A study of micro-channel size and spatter dispersion for laser beam micro-milling," *Materials and Manufacturing Processes*, vol. 32, no. 2, pp. 171-184, 2017.
- [51] J. Chen, X. Zhou, S. Lin, and Y. Tu, "A prediction-correction scheme for microchannel milling using femtosecond laser," *Optics and Lasers in Engineering*, vol. 91, pp. 115-123, 2017.
- [52] C.-W. Cheng, X.-Z. Tsai, and J.-S. Chen, "Micromachining of stainless steel with controllable ablation depth using femtosecond laser pulses," *The International Journal of Advanced Manufacturing Technology*, vol. 85, pp. 1947-1954, 2016.
- [53] S. S. Singh, P. K. Baruah, A. Khare, and S. N. Joshi, "Effect of laser beam conditioning on fabrication of clean micro-channel on stainless steel 316L using second harmonic of Q-switched Nd: YAG laser," *Optics & Laser Technology*, vol. 99, pp. 107-117, 2018.
- [54] Y. Liu, L. Liu, J. Deng, R. Meng, X. Zou, and F. Wu, "Fabrication of micro-scale textured grooves on green ZrO₂ ceramics by pulsed laser ablation," *Ceramics International*, vol. 43, no. 8, pp. 6519-6531, 2017.
- [55] A. Garcia-Giron, D. Sola, and J. Peña, "Liquid-assisted laser ablation of advanced ceramics and glass-ceramic materials," *Applied Surface Science*, vol. 363, pp. 548-554, 2016.
- [56] Y. Zhang, Y. Wang, J. Zhang, Y. Liu, X. Yang, and Q. Zhang, "Micromachining features of TiC ceramic by femtosecond pulsed laser," *Ceramics International*, vol. 41, no. 5, pp. 6525-6533, 2015.
- [57] B. Adelman and R. Hellmann, "Rapid micro hole laser drilling in ceramic substrates using single mode fiber laser," *Journal of Materials Processing Technology*, vol. 221, pp. 80-86, 2015.
- [58] J. Zhang, Y. Long, S. Liao, H.-T. Lin, and C. Wang, "Effect of laser scanning speed on geometrical features of Nd: YAG laser machined holes in thin silicon nitride substrate," *Ceramics international*, vol. 43, no. 3, pp. 2938-2942, 2017.
- [59] V. Soundararajan and V. Radhakrishnan, "An experimental investigation on the basic mechanisms involved in ultrasonic machining," *International Journal of Machine Tool Design and Research*, vol. 26, no. 3, pp. 307-321, 1986.
- [60] R. Singh and J. Khamba, "Ultrasonic machining of titanium and its alloys: a review," *Journal of materials processing technology*, vol. 173, no. 2, pp. 125-135, 2006.

- [61] E. L. Stevens, J. Toman, A. C. To, and M. Chmielus, "Variation of hardness, microstructure, and Laves phase distribution in direct laser deposited alloy 718 cuboids," *Materials & design*, vol. 119, pp. 188-198, 2017.
- [62] V. Popovich, E. Borisov, A. Popovich, V. S. Sufiiarov, D. Masaylo, and L. Alzina, "Impact of heat treatment on mechanical behaviour of Inconel 718 processed with tailored microstructure by selective laser melting," *Materials & Design*, vol. 131, pp. 12-22, 2017.
- [63] R. Ding, Z. Huang, H. Li, I. Mitchell, G. Baxter, and P. Bowen, "Electron microscopy study of direct laser deposited IN718," *Materials Characterization*, vol. 106, pp. 324-337, 2015.
- [64] A. Strondl, R. Fischer, G. Frommeyer, and A. Schneider, "Investigations of MX and γ'/γ "precipitates in the nickel-based superalloy 718 produced by electron beam melting," *Materials Science and Engineering: A*, vol. 480, no. 1-2, pp. 138-147, 2008.
- [65] F. Müller and J. Monaghan, "Non-conventional machining of particle reinforced metal matrix composite," *International Journal of Machine Tools and Manufacture*, vol. 40, no. 9, pp. 1351-1366, 2000.
- [66] Z. Yuan, B. Fang, Y. Zhang, and F. Wang, "Effect of cutting parameters on chips and burrs formation with traditional micromilling and ultrasonic vibration assisted micromilling," *The International Journal of Advanced Manufacturing Technology*, pp. 1-14, 2022.
- [67] A. Muhammad, M. Kumar Gupta, T. Mikołajczyk, D. Y. Pimenov, and K. Giasin, "Effect of tool coating and cutting parameters on surface roughness and burr formation during micromilling of inconel 718," *Metals*, vol. 11, no. 1, p. 167, 2021.
- [68] I. ISO, "International Standard ISO 8688: Tool-life Testing in milling," 1989.
- [69] I. ISO, "8688-2: 1989_Tool life testing in milling—Part 2: End milling," *International Organization for Standardization. ISO*, 1989.
- [70] T. R. Thomas, *Rough surfaces*. World Scientific, 1998.
- [71] D. J. Whitehouse, *Handbook of surface metrology*. Routledge, 2023.
- [72] B. Bhushan, *Principles and applications of tribology*. John Wiley & Sons, 1999.
- [73] B. Bhushan, "Handbook of micro/nano tribology," *Micro/Nanotribology and Micro/Nanomechanics of Magnetic Storage Devices and MEMS*, pp. 443-503, 1995.
- [74] S. Sartori, L. Moro, A. Ghiotti, and S. Bruschi, "On the tool wear mechanisms in dry and cryogenic turning Additive Manufactured titanium alloys," *Tribology International*, vol. 105, pp. 264-273, 2017.
- [75] A. Malakizadi, H. Gruber, I. Sadik, and L. Nyborg, "An FEM-based approach for tool wear estimation in machining," *Wear*, vol. 368, pp. 10-24, 2016.
- [76] Z. Pálmai, "Proposal for a new theoretical model of the cutting tool's flank wear," *Wear*, vol. 303, no. 1-2, pp. 437-445, 2013.
- [77] J. MATUSZAK and K. ZALESKI, "Effect of milling parameters upon burr formation during AZ91 HP magnesium alloy face milling," *NEW MATERIALS NEW MATERIALS AND IT TECHNOLOGIES D IT TECHNOLOGIES D IT TECHNOLOGIES IN PRODUCTION ENGINEERING IN PRODUCTION ENGINEERING*, p. 31, 2011.
- [78] S.-L. Ko and D. A. Dornfeld, "A study on burr formation mechanism," 1991.

- [79] L. Gillespie, "The battle of the burr: new strategies and new tricks," *Manufacturing Engineering(USA)*, vol. 116, no. 2, pp. 69-70, 1996.
- [80] H. I. Kurt, M. Oduncuoglu, N. F. Yilmaz, E. Ergul, and R. Asmatulu, "A comparative study on the effect of welding parameters of austenitic stainless steels using artificial neural network and Taguchi approaches with ANOVA analysis," *Metals*, vol. 8, no. 5, p. 326, 2018.
- [81] K. Nandagopal and C. Kailasanathan, "Analysis of mechanical properties and optimization of gas tungsten Arc welding (GTAW) parameters on dissimilar metal titanium (6Al4V) and aluminium 7075 by Taguchi and ANOVA techniques," *Journal of Alloys and Compounds*, vol. 682, pp. 503-516, 2016.
- [82] S. Pandiarajan, S. S. Kumaran, L. Kumaraswamidhas, and R. Saravanan, "Interfacial microstructure and optimization of friction welding by Taguchi and ANOVA method on SA 213 tube to SA 387 tube plate without backing block using an external tool," *Journal of Alloys and Compounds*, vol. 654, pp. 534-545, 2016.
- [83] M. Satheesh and J. Dhas, "Multi Objective Optimization of Weld Parameters of Boiler Steel Using Fuzzy Based Desirability Function," *Journal of Engineering Science & Technology Review*, vol. 7, no. 1, 2014.
- [84] S. Panda, D. Mishra, and B. B. Biswal, "Determination of optimum parameters with multi-performance characteristics in laser drilling—a grey relational analysis approach," *The International Journal of Advanced Manufacturing Technology*, vol. 54, no. 9-12, pp. 957-967, 2011.
- [85] V. Modi and D. Desai, "Review of Taguchi method, design of experiment (DOE) & analysis of variance (ANOVA) for quality improvements through optimization in foundry," *vol*, vol. 5, pp. 184-194, 2018.
- [86] J. A. Ghani, H. Jamaluddin, M. N. Ab Rahman, and B. M. Deros, "Philosophy of Taguchi approach and method in design of experiment," *Asian Journal of Scientific Research*, vol. 6, no. 1, p. 27, 2013.
- [87] C. Sun, H. Wang, G. Shang, and J. Du, "Parameters optimization for piezoelectric harvesting energy from pavement based on Taguchi's orthogonal experiment design," *World Journal of Engineering and Technology*, vol. 3, no. 04, p. 149, 2015.
- [88] E. Kuram and B. Ozcelik, "Optimization of machining parameters during micro-milling of Ti6Al4V titanium alloy and Inconel 718 materials using Taguchi method," *Proceedings of the Institution of Mechanical Engineers, Part B: Journal of Engineering Manufacture*, vol. 231, no. 2, pp. 228-242, 2017.
- [89] S. H. I. Jaffery, M. Khan, L. Ali, and P. T. Mativenga, "Statistical analysis of process parameters in micromachining of Ti-6Al-4V alloy," *Proceedings of the Institution of Mechanical Engineers, Part B: Journal of Engineering Manufacture*, vol. 230, no. 6, pp. 1017-1034, 2016.
- [90] K. H. Hashmi, G. Zakria, M. B. Raza, and S. Khalil, "Optimization of process parameters for high speed machining of Ti-6Al-4V using response surface methodology," *The International Journal of Advanced Manufacturing Technology*, vol. 85, pp. 1847-1856, 2016.
- [91] E. Ostertagová and O. Ostertag, "Methodology and Application of One-way ANOVA," *American Journal of Mechanical Engineering*, vol. 1, no. 7, pp. 256-261, 2013.

- [92] D. C. Montgomery and G. C. Runger, *Applied statistics and probability for engineers*. John Wiley & Sons, 2010.
- [93] M. Alauddin, M. El Baradie, and M. Hashmi, "Computer-aided analysis of a surface-roughness model for end milling," *Journal of materials processing technology*, vol. 55, no. 2, pp. 123-127, 1995.
- [94] W. Y. Bao and I. Tansel, "Modeling micro-end-milling operations. Part I: analytical cutting force model," *International Journal of Machine Tools and Manufacture*, vol. 40, no. 15, pp. 2155-2173, 2000.
- [95] M. Durante, A. Formisano, and A. Langella, "Comparison between analytical and experimental roughness values of components created by incremental forming," *Journal of Materials Processing Technology*, vol. 210, no. 14, pp. 1934-1941, 2010.
- [96] M. Zhang, D. Zhang, D. Geng, Z. Shao, Y. Liu, and X. Jiang, "Effects of tool vibration on surface integrity in rotary ultrasonic elliptical end milling of Ti-6Al-4V," *Journal of Alloys and Compounds*, vol. 821, p. 153266, 2020.
- [97] M. Vahdati, R. Mahdavinejad, S. Amini, A. Abdullah, and K. Abrinia, "Design and manufacture of vibratory forming tool to develop" ultrasonic vibration assisted incremental sheet metal forming" process," *Modares Mechanical Engineering*, vol. 14, no. 11, 2015.
- [98] K. Liu, X. Li, and M. Rahman, "Characteristics of ultrasonic vibration-assisted ductile mode cutting of tungsten carbide," *The International Journal of Advanced Manufacturing Technology*, vol. 35, pp. 833-841, 2008.
- [99] F. Fang, H. Ni, and H. Gong, "Rotary ultrasonic machining of hard and brittle materials," *Nanotechnol Precis Eng*, vol. 12, no. 3, pp. 227-234, 2014.
- [100] P. M. Mahaddalkar and M. H. Miller, "Force and thermal effects in vibration-assisted grinding," *The International Journal of Advanced Manufacturing Technology*, vol. 71, pp. 1117-1122, 2014.
- [101] A. Mian, N. Driver, and P. Mativenga, "Identification of factors that dominate size effect in micro-machining," *International Journal of Machine Tools and Manufacture*, vol. 51, no. 5, pp. 383-394, 2011.
- [102] C. Ni, L. Zhu, and Z. Yang, "Comparative investigation of tool wear mechanism and corresponding machined surface characterization in feed-direction ultrasonic vibration assisted milling of Ti-6Al-4V from dynamic view," *Wear*, vol. 436, p. 203006, 2019.
- [103] G. Li, B. Wang, J. Xue, D. Qu, and P. Zhang, "Development of vibration-assisted micro-milling device and effect of vibration parameters on surface quality and exit-burr," *Proceedings of the Institution of Mechanical Engineers, Part B: Journal of Engineering Manufacture*, vol. 233, no. 6, pp. 1723-1729, 2019.
- [104] K.-M. Li and S.-L. Wang, "Effect of tool wear in ultrasonic vibration-assisted micro-milling," *Proceedings of the Institution of Mechanical Engineers, Part B: Journal of Engineering Manufacture*, vol. 228, no. 6, pp. 847-855, 2014.
- [105] M. Hanif, W. Ahmad, S. Hussain, M. Jahanzaib, and A. H. Shah, "Investigating the effects of electric discharge machining parameters on material removal rate and surface roughness on AISI D2 steel using RSM-GRA integrated approach," *The International Journal of Advanced Manufacturing Technology*, vol. 101, pp. 1255-1265, 2019.

- [106] D. Biermann and M. Steiner, "Analysis of micro burr formation in austenitic stainless steel X5CrNi18-10," *Procedia Cirp*, vol. 3, pp. 97-102, 2012.
- [107] A. K. Yadav, V. Bajpai, N. K. Singh, and R. K. Singh, "FE modeling of burr size in high-speed micro-milling of Ti6Al4V," *Precision Engineering*, vol. 49, pp. 287-292, 2017.
- [108] Z. Wang, V. Kovvuri, A. Araujo, M. Bacci, W. Hung, and S. Bukkapatnam, "Built-up-edge effects on surface deterioration in micromilling processes," *Journal of Manufacturing Processes*, vol. 24, pp. 321-327, 2016.
- [109] I. Uzun, K. Aslantas, and F. Bedir, "An experimental investigation of the effect of coating material on tool wear in micro milling of Inconel 718 super alloy," *Wear*, vol. 300, no. 1-2, pp. 8-19, 2013.
- [110] X. Lu, H. Zhang, Z. Jia, Y. Feng, and S. Y. Liang, "Cutting parameters optimization for MRR under the constraints of surface roughness and cutter breakage in micro-milling process," *Journal of Mechanical Science and Technology*, vol. 32, pp. 3379-3388, 2018.
- [111] H. Tebassi, M. Yallese, R. Khettabi, S. Belhadi, I. Meddour, and F. Girardin, "Multi-objective optimization of surface roughness, cutting forces, productivity and Power consumption when turning of Inconel 718," *International Journal of Industrial Engineering Computations*, vol. 7, no. 1, pp. 111-134, 2016.
- [112] S. Sreeram, A. S. Kumar, M. Rahman, and M. Zaman, "Optimization of cutting parameters in micro end milling operations in dry cutting condition using genetic algorithms," *The International Journal of Advanced Manufacturing Technology*, vol. 30, pp. 1030-1039, 2006.
- [113] P. Abhilash and D. Chakradhar, "Multi-response optimization of wire EDM of Inconel 718 using a hybrid entropy weighted GRA-TOPSIS method," *Process Integration and Optimization for Sustainability*, pp. 1-12, 2022.
- [114] M. O. Esangbedo and J. K. Abifarin, "Cost and quality optimization taguchi design with grey relational analysis of halloysite nanotube hybrid composite: CNC machine manufacturing," *Materials*, vol. 15, no. 22, p. 8154, 2022.
- [115] M. Sultana and N. R. Dhar, "Hybrid GRA-PCA and modified weighted TOPSIS coupled with Taguchi for multi-response process parameter optimization in turning AISI 1040 steel," *Archive of Mechanical Engineering*, pp. 23-49-23-49, 2021.
- [116] C. M. Rao, K. V. Subbaiah, and C. Suresh, "Optimization of Cutting Parameters Using Weighted Principal Component Analysis (WPCA) Combined with Grey Relational Analysis (GRA) While Turning of AA7075," *International Journal of Hybrid Information Technology*, ISSN, pp. 1738-9968, 2017.
- [117] G. R. Chate, G. M. Patel, R. M. Kulkarni, P. Vernekar, A. S. Deshpande, and M. B. Parappagoudar, "Study of the effect of nano-silica particles on resin-bonded moulding sand properties and quality of casting," *Silicon*, vol. 10, pp. 1921-1936, 2018.
- [118] C.-F. J. Kuo and T.-L. Su, "Optimization of multiple quality characteristics for polyether ether ketone injection molding process," *Fibers and Polymers*, vol. 7, pp. 404-413, 2006.
- [119] M. Sarıkaya and A. Güllü, "Multi-response optimization of minimum quantity lubrication parameters using Taguchi-based grey relational analysis in turning of

- difficult-to-cut alloy Haynes 25," *Journal of Cleaner Production*, vol. 91, pp. 347-357, 2015.
- [120] K. Palanikumar, B. Latha, V. Senthilkumar, and J. P. Davim, "Analysis on drilling of glass fiber–reinforced polymer (GFRP) composites using grey relational analysis," *Materials and manufacturing Processes*, vol. 27, no. 3, pp. 297-305, 2012.
- [121] R. Kumar, P. S. Bilga, and S. Singh, "Multi objective optimization using different methods of assigning weights to energy consumption responses, surface roughness and material removal rate during rough turning operation," *Journal of cleaner production*, vol. 164, pp. 45-57, 2017.
- [122] G. E. Box, J. S. Hunter, and W. G. Hunter, "Statistics for experimenters," in *Wiley series in probability and statistics*: Wiley Hoboken, NJ, 2005.
- [123] A. I. Khuri and S. Mukhopadhyay, "Response surface methodology," *Wiley Interdisciplinary Reviews: Computational Statistics*, vol. 2, no. 2, pp. 128-149, 2010.
- [124] M. G. Kulkarni and A. K. Dalai, "Waste cooking oil an economical source for biodiesel: a review," *Industrial & engineering chemistry research*, vol. 45, no. 9, pp. 2901-2913, 2006.
- [125] T. Hastie, R. Tibshirani, J. H. Friedman, and J. H. Friedman, *The elements of statistical learning: data mining, inference, and prediction*. Springer, 2009.
- [126] J. Cohen, P. Cohen, S. G. West, and L. S. Aiken, *Applied multiple regression/correlation analysis for the behavioral sciences*. Routledge, 2013.
- [127] M. V. Ramana, G. K. M. Rao, and D. H. Rao, "Multi objective optimization of process parameters in turning of Ti-6Al-4V alloy," *Materials Today: Proceedings*, vol. 5, no. 9, pp. 18966-18974, 2018.
- [128] M. Younas *et al.*, "Multi-objective optimization for sustainable turning Ti6Al4V alloy using grey relational analysis (GRA) based on analytic hierarchy process (AHP)," *The International Journal of Advanced Manufacturing Technology*, vol. 105, pp. 1175-1188, 2019.

Certificate for Plagiarism

It is certified that MS Thesis Titled "Laser-based Ultrasonic Assisted Low Speed Micro Milling of Super Alloys" by Mr. Yadullah Haidary, Regn. No. 00000318519 has been examined by us.

We undertake the follows:

- a. Thesis has significant new work/knowledge as compared to already publish or is under consideration to be published elsewhere. No sentence, equation, diagram, table, paragraph or section has been copied verbatim from previous work unless it is placed under quotation marks and duly referenced.
- b. The work presented is original and own work of the author (i.e. there is no plagiarism). No ideas, processes, results or words of others have been presented as Author own work.
- c. There is no fabrication of data or results which have been compiled/analyzed.
- d. There is no falsification by manipulating research materials, equipment or processes, or changing or omitting data or results such that the research is not accurately represented in the research record.
- e. The thesis has been checked using TURNITIN (copy of originality report attached) and found within the limits as per HEC Plagiarism Policy and instructions issued from time to time.

Signature of Supervisor _____

Name of Supervisor: Dr. Syed Husain Imran Jaffery

Dr. Syed Husain Imran
Professor
School of Mechanical and
Manufacturing Engineering
(MSME) NUST, Islamabad